Compressional tectonics and volcanism: the Miocene-Quaternary evolution of the Western Cordillera and Puna Plateau, Central Andes

Jaldin D.[1], Tibaldi A.[2], Bonali F.[2], Giambiagi L[3]., Espinoza D.[4], Luengo K.[1], Santander A.[1], Russo E[2].

[1] Departamento de Ciencias Geológicas, Universidad Católica del Norte, Avenida Angamos, 0610 Antofagasta, Chile
[2] University of Milan Bicocca, Milan, Italy
[3] IANIGLA, CCT Mendoza, CONICET, Mendoza, Argentina
[4] Institut für Geowissenschaften, Universität Potsdam, Potsdam, Germany.

*Correspoding autor. Diego Jaldin, Departamento de Ciencias Geológicas, Universidad Católica del Norte, Avenida Angamos 0610, Antofagasta, Chile. e-mail: djq001@aumnos.ucn.cl , tel. +56 968401854, https://orcid.org/0000-0002-9631-6653

Abstract

The volcanism in compressional tectonic remains several unknows about the relations between faulting, volcano positions and stress field. The Central Andes comprises a one most important volcanic province in the world where this relation is conserved. We investigate the Miocene-Quaternary faulting and tectonic stress evolution in the Western Cordillera between 24°S and 26°S and compare them with the orientation of magma feeding fractures to understand the relations between deformation and volcanism in the Central Andes. We calculated 68 new stress tensors from faults of recognized age and reconstructed magma paths by analyzing the morphostructural characteristics of 130 monogenetic and polygenetic volcanoes of known age. Moreover, we integrated the database with published with previous data from Western Cordillera and Altiplano-Puna further North to carry out a regional comparison. Results allow us to recognize three main volcano-tectonic events. The oldest occurred in the Lower Miocene and was characterized by an E-W greatest principal stress (σ_1) expressed by N-S-striking reverse faults and NW-SE left-lateral strike-slip faults: volcanoes belonging to this stage show morphometric characteristics that indicate dominant N-S magma feeding systems. The second event, active during the Upper Miocene-Pliocene, was characterized by an NW-SE to NNW-SWE σ_1, WNW-ESE right-lateral strike-slip faults, and an NW-SE preferential direction of volcanic feeding systems. The last event was active in the Upper Pliocene-Pleistocene, mainly in the northern part of the study area, with NS to NE-SW normal and right-lateral strike-slip faults with an NNE-SSW-trending least principal stress ($\sigma 3$): volcanism in this stage is characterized by NW-SE and N-S magma feeding systems. Our results suggest that the distributions of volcanoes were mainly controlled by variations of the stress field related to the growth and collapse of the Puna Plateau. Magma emplacement was mostly guided by fractures parallel to the compression direction, irrespective of the horizontal stress being σ_3 or the intermediate principal stress σ_2. The magma emplacement occurred along fractures that strike perpendicularly to σ_1, along strike-slip faults, or by exploitation of inherited weak structures, such as reverse faults.

Key words: stress, volcanism, faulting, Andes

Declaration of competing interest:

The authors declare that they have no known competing financial interests or personal relationships that could have appeared to influence the work reported in this paper.

1. Introduction

A fundamental issue in compressional setting, like the Andes, is how magma reaches the surface. Magma ascent, arrest, storage, or reaching the surface are strongly dependent on magmas properties, as well as on structure and stress state of the host rock (Gudmundsson, 2006, 2012; Chaussard and Amelung, 2014; Tibaldi, 2015). Andean-type tectonics develop in zones of plate convergence, where the maximum principal stress (σ_1) is horizontal and is related to convergence direction (Pardo-Casas and Molnar, 1987). In the Central Andes the stress field resultant produces widespread contraction through the formation and development of reverse faults, fold, and strike-slip fault. Moreover, extensional structures have described associated to orogen collapse (Tibaldi and Bonali, 2018), back arc deformations (e.g. Schoenbohm and Strecker, 2009; Haag et al., 2019; Tye et al., 2022) and how expression to local change in the stress field (Tibaldi et al., 2009; Giambiagi et al., 2016). Associated these faults was development a magmatic arc since late Oligocene distributed along of Western Cordillera and back arc positions (Figure 1)

Contraction environment has been for a long time considered unfavorable to magma upwelling since the position of σ_1 would favor the emplacement of sills, because the least principal stress (σ_3) is vertical (Glazner 1991; Hamilton, 1995; Watanabe et al., 1999). To the magma reach the surface in unfavorable stress field the fluid pressure must be greater than σ3 or σ3<0 (Sibson et al., 1988; Sibson 2004). Indeed, for decades, it has been accredited that volcanism can occur essentially under extensional tectonics, where a horizontal σ_3 and a vertical σ_1 facilitate magma upwelling along vertical fractures perpendicular to σ_3 (Anderson, 1951; Cas and Wright, 1987). Besides, at convergent margins, where compression is expected, Nakamura et al. (1977) and Nakamura and Uyeda (1980) proposed that the stress state should be characterized by horizontal σ_3 and σ_1, corresponding to transcurrent tectonics, with vertical magma paths normal to σ_3.

In the Central Andes, it has been proposed that volcanism was widespread during uplift phases that followed the main shortening events, such as those occurred in Miocene and Plio-Quaternary times in the Altiplano-Puna Volcanic Complex with the emplacement of widespread ignimbrite deposits and several hundreds volcanoes (de Silva, 1989; Trumbull et al., 2006; Kay and Coira, 2009; Ramos, 2009). Uplift is the outcome of crustal thickening, the latter being strictly linked with the contraction event (Isacks, 1988; Kley and Monaldi, 1998; Beck and Zandt, 2002; McQuarrie, 2002). As an example, based on stable isotope data, Ghosh et al. (2006) and Garzione et al. (2006, 2008) indicate that the average elevation in the Altiplano of the Central Andes was about 2 km a.s.l before the Miocene, and then increased to about 2.5 km a.s.l at 10–6 Ma, suggesting that the major uplift phase followed the contraction event at 10 Ma (Eichelberger et al., 2015). Tibaldi (2008) proposed that in contractional settings magma can follow a reverse fault plane in the uppermost crust and then uprise across the volcanic cone through splay faults with a strike parallel to the underlying reverse fault, which is to say along a plane striking perpendicularly to the local σ_1. Possible magma rise along inclined reverse faults has also been confirmed by analogue modelling by Galland et al. (2007a), as well as by geophysical data (Barrionuevo et al., 2019). This orientation of dykes striking perpendicularly to σ_1 has been observed in contractional settings also in the interior of folds (Kruger and Kisters, 2016; Gürer et al., 2016). Additionally, it has been proposed that, in contractional settings, magma rises along planes that are parallel to the shortening direction due to the local development of extensional fractures, as at the Tromen volcano in Argentina (Galland et al., 2007b; Llambías et al., 2011), or at Spanish Peaks, Colorado, USA, where dykes parallel to the shortening direction have been interpreted as due to the interference between a regional stress state with horizontal σ_1 and σ_3 and an overpressurized central conduit (Odé, 1957; Johnson, 1970; Nakamura, 1977). Ruch and Walter (2010) proposed Lazufre magmatic body rise throughout two phases first a perpendicular σHmax elongation of magmatic bodies followed to fractured opening parallel to σHmax development in hanging-wall of reverse faulting (Naranjo et al., 2018). Other models of magma rise were proposed extensional activity of reactivated fault (Haag et al., 2019), and extension in transfer zones of NW-SE fault system (Riller et al., 2001; Ramelow et al., 2006; Lanza et al., 2013).

Despite these observations, it remains debatable which are the structures and conditions that allow magma to rise in the uppermost crust. Moreover, since volcanism did occur during the main contraction orogenic, strike-slip and extensional events the discussion about the nature of magma paths under different stress field is still open.

A more in-depth understanding of the geometry of the plumbing system that allows magma to reach the surface, in relation to the acting stress and strain state, is not only fundamental for the comprehension of how volcanoes generally work, but it is also of paramount importance for contributing to the assessment of volcanic hazard. For example, in the Central Andes there are tens of volcanoes in a dormant stage, and their possible awakening can occur with the opening of flank vents; the location of the areas of vent opening depends on the orientation of the magma feeder dyke, whose comprehension is thus of direct application (Bonali et al., 2011; Tadini et al., 2014).

In the Central Andes, only one study has been devoted to a detailed comparison, between magma feeder dykes and the tectonic evolution of the region (Tibaldi et al., 2017). As a matter of fact, the lack of this type of work in the area is mainly related to the rarity of outcropping Neogene-Quaternary dykes that might give direct clues on the plumbing system, to the absence of shallow geophysical data, and to the logistical difficulty of the region, which is characterized by volcanoes mostly located in hardly accessible, remote areas. In the present work, we analyze a wide Andes region, located between 24°S and 26°S to the south of the area studied by Tibaldi et al. (2017), and, as a next step, we integrate and compare our data with their data and with structural data from Tibaldi et al., (2009) and Giambiagi et al., (2016) (Figure 1). This allows to discuss the relations between faulting, stress state and magma feeder paths in an area of 12,720 sq km between 19°S and 26°S of western Cordillera, representing a significant portion of the Central Andes. We present new data collected mainly in the field, focusing on the Miocene-Pliocene-Quaternary evolution of faulting, distinguishing the main phases, kinematics and strain. Furthermore, we show the evolution of the stress state after processing the data on striated fault planes with calculation of the stress tensor for a fault population of given age. Finally, we compare the structures and stress field with the orientation of magma feeder fractures, referring to 130 volcanoes of different ages. The orientation of the shallow magma paths has been reconstructed by using a series of morphometric indicators measured on each single volcanic edifice; this is a method firstly proposed by Tibaldi (1995), and then consolidated by Corazzato and Tibaldi (2006), Kervyn et al. (2012), Germa et al. (2013) and Hernando et al. (2014). Results allow to delineate the complete evolution of tectonics and volcanism in the studied area, and more generally, indicate how volcano growth, through the magma feeder fracture, can be sensitive to the tectonic stress field or, instead, to the presence of mechanical weakness zones such as faults, or to the interference with folds. These data help to better understand magma ascent in compressional settings.

2. Geological background

The south Central Andes, between 24°S and 26°S, are composed of four regions structurally and geologically different, which are named, from west to east (Fig. 1): 1) Forearc region, which corresponds to the Coastal Cordillera (CC), Central Depression (CD), Domeyko Range (DO), and Pre-Andean Basin (AB) (Figure 1). This region is characterized by several reverse and strike-slip fault systems of long-lived deformations active since the Paleozoic (e.g. Charrier et al., 2007; Mpodozis and Ramos, 2008; Lopez et al., 2019); 2) Western Cordillera (WC), which extends to the Chile-Bolivia and Chile-Argentina borders, and consists of a volcanic chain active since the Upper Oligocene; 3) Altiplano-Puna Plateau (PP), which is a basin with ca. 2000 km of long in N-S and 300 km to width, located in northwestern Argentina and southwestern Bolivia (Almendinger et al., 1997); and 4) the eastern fold-and-thrust belt composed by the Eastern Cordillera (EC) and the Santa Barbara Range (SB). The current configuration of the Central Andes is the result of superimposed tectono-magmatic processes, which have been active especially in Triassic-Quaternary times (Allmendinger et al., 1997; Charrier et al., 2007; Oliveros et al., 2007).

The study area is located in the Western Cordillera between 24°S and 26°S (Fig. 1). The oldest rock sequences crop-out in the Almeida range, located in the northern part of the study area (Fig. 2) (Solari et al., 2017). These sequences correspond to carbonaceous and siliciclastic units, named Zorritas Formation of Devonian-Carboniferous age, and continental and volcanic sequences of Upper Carboniferous to Lower Cretaceous age, which comprise the Agua Escondida, La Tabla, and Estratos de Cerro de Puquios Formations (Gardeweg et al., 1993; Solari et al., 2017). These formations have been intruded by several granites and hypabyssal intrusive suites, with ages ranging between 298 and 242 Ma (Solari et al., 2017). Mesozoic units, outcrop in the Almeida range, correspond to volcanic and siliciclastic sequences of Triassic and Cretaceous age, represented by the Pular and the Quebrada Pajonales Formation.

Cenozoic sedimentary rocks crop out in a scattered way: they have been deposited in the Puntas Negras Basin since the Paleocene-Oligocene and are mostly covered by volcanic sequences of Early Miocene and Late Miocene age (Villa et al., 2019). In the southern part of the study area, the upper Oligocene and Lower Miocene siliciclastic sequence of Quebrada Tocomar Formation is interbedded with the Rio Frio ignimbrite, which has been dated between 23 and 16 Ma (Gardeweg et al., 1993). These sequences form a high plateau covered by the Miocene to present volcanic deposits of the modern volcanic arc. This Miocene-Quaternary volcanism, started at ca. 23 Ma (Naranjo et al., 2013 a,b; 2018 a), is composed by several andesite stratovolcanoes, dacitic and rhyolitic domes, basaltic and scoria cones, isolated pyroclastic flows, and comprises caldera structures largely preserved by the arid climatic conditions of the area. From the geochronological datings by the Chilean Geological Service (Naranjo et al., 2013a, b; Solari et al., 2017; Villa et al., 2019), the evolution of the volcanic arc can be divided into four stages. The first stage includes volcanic deposits erupted between 20 and 14 Ma: these products are distributed in the southern part of the study area, along the corridor of the NW-oriented Culampaja Lineament and in isolated volcanoes in the central part (Fig. 2). The second stage, with ages between 14 and 9 Ma, is characterized by products mainly present along the Culampaja Lineament and concentrated in the central part of the study area around the Pajonales Salar (Fig. 2). The third stage, active from 9 to 3 Ma, represents the widest areal distribution of volcanism and is concentrated in the central part of the study area with a general NNE-SSW volcanoes range. The last stage considers rocks from 3 Ma to the current volcanic activity: these deposits are located in narrowly-defined positions in the central part of the study area, and are represented by Lastarria volcanoes and Cordon Azufre Volcanic Chain, which corresponds to the long-lived Lazufre magmatic-bodies (Naranjo et al., 2018a). Moreover, in the northern part by Llullaillaco volcano (Fig. 2).

The Cenozoic tectonic evolution of the Central Andes was dominated by continuous compression (DeCelles and Horton, 2003; Deeken et al., 2006; Strecker et al., 2007) caused by the convergence between the Nazca and the South American plates (Pardo Casas and Molnar, 1987, Somoza and Guidella, 2012). The compression, mostly perpendicular to the orogen, caused shortening, which lead to the formation of the Andean Altiplano-Puna Plateau (Allmendinger et al, 1997). The contractional deformation onset in the Late Cretaceous produced the tectonic inversion of Mesozoic basins, and deformations registered in the Domeyko Fault system and Coastal Cordillera (Mpodozis et al., 2005; Bascuñan et al., 2015). This contractional deformation continued forming reverse and transpressional faulting in the Eocene-Oligocene (Jordan et al., 1987; Kraemer et al., 1999; Coutand et al., 2001; Carrapa et al., 2005; Mpodozis et al., 2005). The Neogene to Present contractional deformation is especially concentrated in the back-arc position (Marrett et al., 1994; McQuarry et al., 2005). Based on geochronological data, the compression in the Altiplano-Puna Plateau ceased at 9-10 Ma and migrated to a more eastern position in the fold-and-thrust belt (Gubbels et al., 1993; Clodouhos et al., 1994; Baby et al., 1995; Moretti et al., 1996; Echavarria et al., 2003). However, contractional deformation in Miocene-Quaternary times has been described in the Western Cordillera that affected the Neogene volcanic deposits (Gonzalez et al., 2009; Naranjo et al., 2018b). This compressional history is well represented by the Guanaqueros-Almeidas fault (Fig. 2), which corresponds to a reverse fault active from the Eocene to the Miocene (Villa et al., 2019), and by the Arizaro-Pedernales fault, interpreted by Naranjo et al., (2018b) as a reverse, east vergent fault, active in the Upper Miocene-Quaternary.

Other faults related to the Cenozoic evolutions of the Central Andes are represented by NW-striking strike-slip faults (Salfity, 1985; Marret et al., 1994; Viramonte et al., 1984; Riller et al., 2001), which are mainly present in the Altiplano-Puna Plateau and have been extended in the Western Cordillera and Domeyko range by Richards and Villanueve (2002) and Yañez and Rivera (2019). The presence of strike-slip systems, oblique with respect to the Western Cordillera trend, is related to the reactivation of inherited crustal discontinuities (Schoenbohm and Strecker, 2009; Lanza et al., 2013, Riller et al., 2001), and alternatively, could be explained by slip partitioning resulting from oblique plate convergence (Pardo Casa and Molnar, 1987; Cladouhos et al., 1994). The activity of this fault system is related to the presence and development of magmatism in the forearc and the entrapment of magmatic bodies (Yañez and Rivera, 2019). In the volcanic arc and back arc positions the Neogene activity of the NW fault system controlled the presence of calderas and volcanic centers (Screiber and Shawab 1991; Riller et al., 2001; Matteini et al., 2002; Ramelow et al., 2006; Bonali et al., 2012; Lanza et al., 2013; Norini et al., 2013; Richard and Villeneuve 2002).

Moreover, extension-related normal faulting has been described in the Central Andes, as distributed mainly in the Altiplano-Puna Plateau, and locally in the Western Cordillera. Normal faults have two main orientations: parallel and perpendicular to the orogen (Allmendinger, 1986; Allmendinger et al., 1989; Marret et al., 1994; Daxberger and Riller, 2015). In the Western Cordillera, an extensional regime has been suggested, related to caldera formation and emplacement of related ignimbrite deposits (Naranjo et al., 2018a). In the study area, the most prominent extensional structures are related to the Aguilar Caldera Formation, between 19 and 17 Ma (Naranjo et al., 2018a) and to the Salar Grande Caldera, active between 13 and 11.5 Ma (Naranjo and Cornejo, 1992; Schnurr et al., 2007; Naranjo et al., 2018a).

The Neogene-Quaternary normal fault parallel to the plate margin in the Altiplano-Puna Plateau and Western Cordillera has been interpreted as due to the formation of footwall synclines and hanging-wall anticlines with bending moment extension (Daxberger et al., 2015). Instead, extension orthogonal to the trench has been explained by the development of fractures locally conjugated to the main compressive stress (Naranjo et al., 2018b). Additionally, extension has also been interpreted as the local effect of a large vertical stress linked to high topography, since normal faults are mainly present at the highest altitudes (Tibaldi et al., 2009; Bonali et al., 2012; Giambiagi et al., 2016). Based on these authors, the local change of the stress field in the Central Andes is expressed by a variation from reverse to strike-slip faulting and finally to local normal faulting and is related to lateral growth and subsequent orogenic collapse.

3. Methodology

3.1. Structural evolution

In order to determine the various stages of deformation that affected the study area, we performed a new field structural mapping at 1:50,000 scale, which was integrated with already published geological data (Naranjo et al., 2013a, 2013b; Venegas et al., 2013; Solari et al., 2017; Villa et al., 2019). The data collected in this study are represented in three maps (location in Fig. 2): Sierra de Almeida (Fig. 4), Aguas Calientes (Fig. 6), and Culampaja (Fig. 7). The main structures exposed in each area were firstly recognized on satellite images, using Google Earth software, and by the analysis of digital elevation models with 12.5 m of spatial resolution obtained from ALOS-Palsar imagery sources available from the ALASKA-VERTEX service (https://search.asf.alaska.edu). Successively, these structures were checked in the field, and their ages were inferred through stratigraphic relations. Structural mapping comprises the assessment of fault slip indicators obtained from field analyses of the main fault planes, and their subsidiary planes. Moreover, we measured the attitude of Cenozoic deposits to characterize fold structures. The field data was complemented with the data obtained unpublished work by Crignola (2002). With these data we performed detailed kinematic analysis and represented in stereographic plot, from which were obtained P and T axis and movement planes. The kinematic analysis was made with fault slip-data (n = 914) obtained from mesoscale faults recognized in pre-Neogene sequences and in Neogene volcanic deposits (Supplementary information 1). The data were obtained at 61 structural stations, of which 20 are distributed in deposits belonging to the Almeida Domain, 23 in the Aguas Calientes Domain, and 18 in the Culampaja Domain (Supplementary information 1). We used the classical indicator criteria of fault slip of Petit et al. (1987) to determine kinematics.

3.2 Strain and stress analyses

The principal strain axes were computed using the Linked Bingham method implemented in Faultkin 8 software (Allmendinger, 2018). More in detail, we calculated the principal strain axes of shortening (**λ** 3) and extension (**λ** 1) and the movement plane. We identified different subset data from the heterogenous distributions based on the grouping of tension axes (T) and pression axes (P), geological field observations, and cross-cutting relations between fault planes.

In order to characterize the folds present in the Miocene-Pliocene volcanic and sedimentary rocks, we performed a stereographic analysis of S0 bending. The data were adjusted with a cylindrical best fit, and the shortening axes were obtained through Bingham axial distribution method; the analysis was performed in Stereonet 10 (Allmendinger et al., 2011).

After dividing the data throgouth kinematic analysis and field observations, we calculated reduced stress tensors to estimate paleostresses, considering that rock ages were known, and the age of deformation was delimited. We performed a paleostress inversion using “Structural geology to Post-Script converter” (SG2PS, Sasvári and Baharev, 2014), based on a computation proposed by Angelier (1990). From this analysis, we obtained 68 reduced stress tensors with positions of the principal axes (σ_1, σ_2, and σ_3), and the stress ratio $\phi= (\sigma_2 - \sigma_3)/(\sigma_1 - \sigma_3)$ for Neogene deformations (Table 1): each tensor was obtained from sites with an average of 13 data, and a minimum of 7. Additionally, we used stress index R’ (Delvaux et al., 1997) to numerically characterize the stress regime. With this index, the authors classified the solution in radial extension (0<R’<0.25), pure extension (0.25<R’<0.75), transtension (0.75<R’<1.25); pure strike/slip (1.25<R’<1.75); transpression (1.75<R’<2.25), pure compression (2.25<R’<2.75); radial compression (2.75<R’<3).

The stress tensor interpretation is a powerful tool; however, it should be studied with caution (Lacombe, 2012). As a consequence, we measured mesoscale faults with many different orientations (Kaven et al., 2011), considering the assumption that parallelism between shear and slip vectors on a fault plane could be affected by several external factors (Twiss and Unruh, 1998, Maerten et al., 2000, Kaven et al., 2011), which comprise mechanical and kinematic interactions between faults (Pollard and Segall, 1987; Dupin et al., 1993; Maerten, 2000), anisotropy defined by the asymmetry of the fault system (Maerten et al., 2000) or preexisting planes of weakness (Marrett and Allmendinger, 1994; Nieto-Samaniego, 1999; Martinez-Díaz, 2002), rotations of blocks bounded by faults (Twiss and Unruh, 1998; Gapais et al., 2000), and perturbations in the stress field produced by fault slip at tips (Pollard and Segall, 1987; Aydin and Schultz, 1990; Barton and Zoback, 1994; Willemse, 1997; Maerten et al., 2000). Moreover, we assumed that the analyzed rocks are mechanically isotropic, and that the stress tensor is homogenous and temporally constant during the fault event.

3.3 Reconstruction of magma feeding fractures

All volcanoes in the study area were grouped into four age classes based on existing radiometric data (Naranjo et al., 2013a, 2013b; Venegas et al., 2013; Gonzalez et al., 2015; Solari et al., 2017; Villa et al., 2019). More in detail, volcanoes were grouped into 1) Lower Miocene (23-11 Ma); 2) Upper Miocene (11-5 Ma); 3) Pliocene (5-2.6 Ma); 4) Pleistocene-Holocene (< 2.6 Ma). For volcanoes lacking radiometric data, we used a comparative morphological approach, consisting in assigning a relative age by comparing lava texture, degree of erosion and hydrothermalization with respect to dated volcanoes. These observations result from the integration of published geological maps, field surveys and remote-sensing observations from Google Earth and digital elevation models. These observations where consistent with age assigned for Chilean Geological services, SERNAGEOMIN (Naranjo et al., 2013a, 2013b; Venegas et al., 2013; Gonzalez et al., 2015; Solari et al., 2017; Villa et al., 2019).

The reconstruction of magma feeding paths, based on volcanoes morphometric data is necessary in areas where dykes do not crop out due to the presence of recent volcanoes, of an extensive cover of epiclastic and volcanic deposits, or to very low erosion rate, all characteristics typical of the Central Andes. The reconstruction is an indirect method that allows to assess the most plausible orientation of the shallow magma-feeding fracture. We used the methodology proposed for pyroclastic cones (Settle, 1979; Pasquarè et al., 1988; Tibaldi et al., 1989; Tibaldi, 1995; Corazzato and Tibaldi, 2006; Paulsen and Wilson, 2010), for volcanic domes (Pasquarè and Tibaldi, 2003) and Polygenic edificies (Nakamura, 1977; Nakamura et al., 1977). Since the volcano morphometric characteristics can be influenced by the dip of the substrate topography, it is necessary to inspect the substrate inclination around the cone, which should be < 9° (more details can be found in Tibaldi, 1995). Thus, in the study area, we measured at each cone the substrate inclination, and considered only those edifices that rest upon a topography with an average inclination lower than 9°. Furthermore, particular attention was given to cones growing on the flank of, or nearby, a pre-existing volcano, because this setting can influence the morphology of the younger cone.

In total we selected 440 volcanoes, comprising both polygenic and monogenic edifices. Then we measure directional parameters for each volcano recognized. We used morphometric parameters that better suggest the shallow magma-feeding fracture, following the indications by Tibaldi (1995) and Corazzato and Tibaldi (2006). These parameters are: i) in the case of well-preserved landforms, the azimuth orientation of crater elongation, ii) in case the cone base limit is not obscured by more recent deposits, the azimuth orientation of cone-base elongation, iii) in the case of presence of different conterminous vents of the same age, the azimuth of the alignment of centre points of the vent/craters, iv) in the case of presence of a well-preserved pyroclastic crater rim, the azimuth of the line connecting the two depressed points, v) the azimuth of elongation of coalescent craters (Figure 3).

These parameters have been extended also to polygenic volcanoes (as done for example by Tibaldi and Bonali, 2017 in the Aleutian Arc) if edifices have well preserved morphostructures. For volcanic domes, we used the azimuth of the apical graben, also known as crease structure (Pasquarè and Tibaldi, 2003). We used Google Earth images, together with Hillshade and RRIMM Images (Chiba et al., 2008), which were obtained from digital elevation models with 12.5 m of spatial resolution, to carry out these measurements.

4. Results

4.1. Miocene-Quaternary faulting

4.1.1 Deformation in the Almeida domain

The Almeida area is located along the border between Western Cordillera and Domeyko range (Fig. 4), where pre-Neogene sequences in contact with Miocene-Quaternary volcanic deposits are present. In this area, Paleozoic and Mesozoic units belong to two chains: Sierra Guanaqueros to the west, and Sierra de Almeida to the east. In the middle, there is an intermontane basin named Quebrada Guanaqueros, which was filled by Miocene alluvial deposits (Solari et al., 2017). We identified two main styles of deformations in the area (Fig. 4): (1) Reverse faulting along N-S to NNE-striking planes, represented by the Pan de Azucar Fault, Fortuna Fault, and the Guanaqueros Fault System; and (2) strike-slip faulting along NW-striking structures, represented by the Sierra de Almeida Fault, Agua Amarga Fault, and Archibarca Fault system.

The Pan de Azucar Fault is a reverse fault with tectonic transport to the east that thrusted Paleozoic formations over Paleocene sequences. The orientation of the shortening axis of this fault, and associated minor faults, is ESE (stereogram E014 in Fig. 4).

In the same way, the Fortuna Fault corresponds to a system of NNW-striking reverse faults with E-W shortening axis (E011b), with uplift of Paleozoic deposits. The mountain front formed by this fault corresponds to the eastern limit of the intermontane basin of Quebrada Guanaqueros, which is filled by the Quebrada Guanaqueros Ignimbrite of 9.9 ± 0.5 Ma (Solari et al., 2017). Moreover, along this mountain front, there is a pediment surface in correspondence with the uppermost part of the Upper Miocene alluvial sequence. Starting from these data, it is possible to obtain the youngest fault activity at ca. 10 Ma.

The Guanaqueros Fault system corresponds to several NNE reverse faults with eastern tectonic transport, and NE-SW to E-W shortening axes. We identified that these reverse faults (E021) rise the Paleozoic sequence, and that the Oligocene-Miocene sequence was deposited in onlap on the back limb of the main thrust (Fig. 5A). Moreover, the same Oligocene-Miocene (18.7 ± 3.6 Ma; Villa et al., 2019) sequence is affected by other reverse faults that form scarps of decametric to a few hundreds meters height (Fig. 5B). At measurement site E131 (Fig. 4), the scarp formed by the reverse activity of Guanaqueros Fault is covered by pyroclastic deposits of 9.9 ± 0.16 Ma (Villa et al., 2019) and forms a barrier to lava flows of the Llullaillaco Volcano of 1.5 ± 0.4 Ma (Gardeweg et al., 1993). According to these data, it is possible to suggest that the Guanaqueros Fault system has been characterized at least by two reverse episodes: the first occurred during pre-Oligocene and is associated to most of the relief formation, and the second was active from 18.7 ± 0.6 Ma until 9.9 ± 0.16 Ma.

The Sierra de Almeida Fault system is characterized by NNW- to NW-striking planes that bound to the E and NE of the Sierra de Almeida. At this fault system, we identified two main deformation episodes: the first corresponds to an approximate E-W shortening, that formed left-lateral (E012, and E114a) strike-slip and reverse faults (E116). This episode affected the Oligocene to Lower Miocene sequence of Pampa de Mulas Formation, dated at 16.3 ± 2.7 Ma (Gardeweg et al., 1993) in the West of Sierra de Almeida. The second episode corresponds to right-lateral strike-slip movements with NW-SE shortening axis (E114b), registered in Paleozoic rocks up to the Upper Miocene alluvial sequence. Locally, Paleocene deposits thrusted over alluvial deposits of Middle Miocene to Pliocene have been observed (9.2 ± 0.8 to 4.7 ± 0.3 Ma, Brook et al., 1986) (Fig. 5D).

The Agua Amarga Fault system corresponds to NW-striking faults located in the central part of Sierra de Almeida. We identified two structural episodes along these faults during the Neogene: the first is characterized by left-lateral strike-slip motions and an ENE-WSW shortening axis (E107a, E106a, E011a), along faults that affect Paleozoic sequences and are covered by Upper Miocene alluvial deposits (9.9 ± 0.5 Ma, Gardeweg et al., 1993) and by Quaternary volcanic deposits (1.4 ± 0.5 Ma, Solari et al., 2017). The second corresponds to right-lateral strike-slip motions and a N-S shortening axis (E107b). The activity of right-lateral strike-slip faults displaced the trace of streams that carved the surface formed by the Upper Miocene to Pliocene sequence (4.7 ± 0.3 Ma; Brook et al.,1986); moreover, fault traces are covered by Quaternary volcanic deposits of 1.4 ± 0.5 Ma (Solari et al., 2017).

The Archibarca Fault system is characterized by several discrete NW-striking faults located to the south of the Guanaqueros Fault, which pass through the Quebrada Las Zorras, the Llullaillaco Volcano and to the south of the Quebrada Guanaqueros basin. The kinematic analysis reveals that this fault system shows left-lateral strike-slip motions that affected the Oligocene to Upper Miocene alluvial sequence (E123c, E005) and volcanic deposits of 16.65 ± 0.06 Ma (E128a) (Villa et al., 2019) and 9.2 ± 0.06 Ma (E129) (Villa et al., 2019). These faults are covered by deposits of a stratovolcano dated at 5.69 ± 0.04 to 4.98 ± 0.5 Ma, south of E130 (Villa et al., 2019). Furthermore, we recognized that right-lateral strike-slip motions affected deposits belonging to stratovolcanoes dated at 15.65 ± 0.06 Ma (E128b), 11.0 ± 0.05 Ma (E126), and 4.98 ± 0.04 Ma (E130) (Villa et al., 2019). At site E128, we observed cross-cutting relations between two sets of striae, where the younger, of right-lateral strike-slip kind, interrupt older left-lateral strike-slip striae (Fig. 5D).

In summary, these structural and kinematic results, obtained in the Sierra de Almeida area, reveal that there have been three main episodes of deformation along the studied fault systems. The first was characterized by reverse faults with the shortening axis trending ~E-W, active during the Lower Miocene (> 12 Ma). The second was represented by left-lateral faults, active during the Middle to Upper Miocene. The third, active since ca. 4 Ma, is characterized by several NW-striking right-lateral strike-slip faults, with N-S to NNE-SSW shortening directions.

4.1.2 Deformation in the Aguas Calientes domain

The Aguas Caliente domain is located in the Western Cordillera, between 24°50´S and 25.15°S (Fig. 6). Here, geological units correspond to a Neogene to Miocene sequence of ignimbrites and other volcanic rocks deposited continuously from the Lower Miocene (17.87 ± 0.07 Ma) to the Quaternary (Villa et al., 2019). In this area, intermontane basins were filled by Pliocene-Quaternary alluvial deposits, formed as a consequence of erosion of volcanic deposits. We identified two principal fault systems in the area: (1) a reverse N-S to NNW-striking system, composed by the Aguas Calientes Fault and several parallel and isolated faults in the central part of the area; and (2) a NW-striking, strike-slip fault system, composed of the Archibarca and Tocomar.

The Aguas Calientes Fault, located along the eastern margin of Aguas Calientes volcano, extends from the southern sector of the Cerros de Tocomar, with a N-S strike, to the south of Aguas Calientes volcano, where it changes strike to NNE-SSW (Fig. 6). Field kinematic data allow us to divide the fault activity in two parts. The first is characterized by reverse faults with east tectonic transport that affect volcanic deposits of 15.71 ± 0.04 Ma (Villa et al., 2019). The scarp formed by the Aguas Calientes Fault is covered by deposits of 12.12 ± 0.17 Ma (Villa et al., 2019) of the Volcan de la Pena. The second comprises the development of left-lateral NNE-SSW strike-slip faults, with a NW-SE shortening axis (E324b, E305b), that cut the volcanic sequences of Volcan de la Pena (12.12 ± 0.7 Ma, Villa et al., 2019). Moreover, during this stage, a fold formed in the eastern flank of Aguas Calientes volcano (13.06 ± 0.07 Ma, Villa et al., 2019), associated with the Archibarca Fault system, that is composed of several NW-striking faults located in the northern part of the area, along the Los Asperos belt (Fig. 6). The kinematic analysis reveals two episodes of activity: the first corresponds to left-lateral strike-slip faulting with E-W (E309) to NE-SW (E317a) shortening axes, a deformation that affected the Lower Miocene volcanic sequence (12.50 ± 0.05 Ma, Villa et al., 2019). The second episode corresponds to NW-SE-striking right-lateral strike-slip faults, with NW-SE (E311b, E319) to NNE-SSW (E310) shortening axes, which affected Upper Miocene deposits (5.68 ± 0.03 Ma, Villa et al., 2019).

The Tocomar Fault system, located in the central part of the study area, extends between the Aguas Calientes volcano and the northern flank of Lastarria volcano: this system is composed of several discontinuous, NW-striking strike-slip faults. Our data reveal two main deformation episodes, which are in agreement with data from the Archibarca fault system. The first corresponds to left-lateral strike-slip faults with E-W (E304a) to ESE-WNW (E320b, E313a) shortening axes, which affect the Lower and Upper Miocene sequence of Aguas Calientes volcano (15.0 ± 0.06 Ma, Villa et al., 2019; 6.1 ± 0.3 Ma to 7.1 ± 0.7 Ma, Naranjo and Cornejo, 1992). The second is characterized by right-lateral strike-slip movements along NW-striking planes with NNW-SSE (E308, E304b, E314) and NE-SW (E320a, E316) shortening axes. The youngest sequence affected by right-lateral faulting has an age of 4.2 ± 0.3 Ma (Naranjo and Cornejo, 1992) and the fault trace is covered by Pleistocene volcanic deposits (1.8 ± 0.5 Ma, Naranjo and Cornejo, 1992). Moreover, it is possible to find reverse, NE-striking faults affecting the Upper Miocene sequence (E312, E318a). Reverse faults have a NNW-SSE shortening axis, coinciding with the right-lateral fault shortening axis: this correlation reveals that reverse faults acted as a transition zone between the NW-striking transcurrent segments of the Tocomar Fault system.

In summary, these results show three main episodes of evolution of the Aguas Calientes domain. In the first, the development of reverse faults occurred, with an E-W shortening axis, represented by the Aguas Calientes Fault system. Afterwards, the left-lateral strike-slip activity of Archibarca and Tocomar fault systems started during Middle Miocene. Finally, the fault activity shifted to right-lateral strike-slip after ca. 4 Ma.

4.1.3 Deformation in the Culampaja domain

The Culampaja domain is located in the southernmost part of the Punta Negra Basin (Fig. 2). This area represents the transition between the Domeyko Range, composed of Paleozoic and Mesozoic rocks, and the Western Cordillera represented by Miocene to Present volcanic arc deposits. The structural observations reveal the presence of two main structural trends. The first corresponds to reverse faults with an approximate N-S strike composed by the Vaquillas and El Chaco faults. The second domain is represented by NW-striking strike-slip faults coinciding with the Culampaja Fault system. In the transition between Culampaja Fault system and Vaquillas fault there is a NNW-SSE fault named Rio Frio Fault.

The Vaquillas Fault is located in the eastern part of the Vaquillas Altas Range. This structure corresponds to an East-directed reverse fault with a E-W shortening axis (E501a). The fault activity produced a decametric scarp in the Rio Frio Ignimbrite (Fig. 5F) that controlled the sedimentation of the Upper Miocene alluvial deposits. These stratigraphic-structural relations allow us to delimit the fault activity between 18.2 ± 0.7 Ma (Naranjo and Cornejo, 1992) and 5.4 ± 1.6 Ma (Gonzalez et al., 2015).

The Chaco Fault corresponds to a reverse fault with an East-tectonic transport and an ENE-WSW shortening axis (E521). The fault affects the Rio Frio Ignimbrite (20.9 ± 1 Ma, Naranjo et al., 2013a) forming a 400-m-high scarp. The scarp is covered by a lava flow of the El Chaco volcano dated between at 17.0 ± 0.7 Ma and 15.0 ± 0.6 Ma (Cornejo and Mpodozis, 1996). Associated with the main scarp, there are several West-directed reverse faults, which thrust the Rio Frio Ignimbrite over the Pajonales Ignimbrite.

The Culampaja Fault system is composed of several discontinuous NW-striking segments and corresponds to strike-slip faults that extend from Vaquillas Altas range to Cerro Leon (Fig. 7). The kinematic analysis reveals two main episodes of deformation; the first corresponds to left-lateral strike-slip faulting (E514b) which affects the volcanic deposits of Upper Miocene age, and it is characterized by an E-W shortening axis. The second episode formed right-lateral strike-slip faults with NW-SE (E505, 518b, 515a) and NNE-SSW (E501b, E512, E522, E514a) shortening axes. This faulting also affects volcanic deposits of 4.7 ± 0.6 Ma (Naranjo et al., 2013a), and the trace of the Culampaja Fault is covered by Quaternary deposits of the Cerro Bayo volcanic complex (1.6 ± 0.4 Ma, Naranjo and Cornejo, 1992).

To sum up, the data of the Culampaja domain show three main episodes of deformation: (1) a contractional episode characterized by reverse faults active during the Lower Miocene; (2) a strike-slip event characterized by NW-oriented left-lateral strike-slip faults active during the Middle Miocene; (3) a strike-slip event characterized by NW-oriented right-lateral strike-slip faulting, active from the Upper Miocene to part of the Pleistocene.

4.2. Miocene-Quaternary Stress

The data described in the previous sections allowed us to divide the tectonic evolution of the Western Cordillera in three main episodes (Lower to Middle Miocene, > 8 Ma BP; Upper Miocene to Pliocene, 8-4 Ma; Upper-Plicoene, < 4 Ma). The different tectonic stresses and the related structures are described in this section.

The reduced stress tensors obtained from the fault population of the first episode (> 8 Ma BP) show a high homogeneity in σ_1 orientations. The rose diagram (Fig. 8A) shows the maximum frequency of orientation of σ_1 in an E-W position (N90°-100°) and few scattered data in ENE-WSW to ESE-WNW orientations (N70°-90°). A second group, with a lower frequency of orientations, has a NE-SW direction. Stress tensors obtained for this episode are located in the western part of the Western Cordillera and correspond to the activity during the Lower Miocene in the Sierra del Almeida, of the Aguas Calientes fault and the first stage of evolution of the Vaquillas and El Chaco faults (Fig. 8A). Eight out of the obtained 26 reduced stress tensors correspond to a pure compressive to radial compressive regime (R'>2.25; Table 1), 5 to transpressive regime (1.75<R'<2.25) and 9 to pure strike-slip regime (1.25<R'<.1.75). The compressive regime is related to reverse activity of Guanaqueros and Aguas Calientes faults, active until ca. 12 Ma. On the other hand, the transpressive to strike-slip regime controlled the activity of the first stage of the Tocomar fault system, which was active until 8 Ma BP. We interpret this as a reduction of relative differences between σ_v (σ_3) and σ_{Hmin} (σ_2), associated to a σ_2/σ_3 permutation. The remaining tensors obtained in this stage show transtension to pure extension, one tensor located south of Sierra de Almeida and two related with activity of Guanaqueros and Fortuna faults (Figure 8A).

In the second episode (8-4 Ma), the directions of reduced stress tensors show a shift of σ_1 from E-W to NW-SE and NNW-SSE positions (Fig. 8B). The rose diagram shows a main NNW-SSE (N150°-160°) σ_1 orientation, followed by a NW-SE orientation (N120°-150°), and a lower NE-SW peak. Orientations of σ_1 are mostly homogeneous and concentrated in the central part of the study area.

The reduced stress tensors (n = 26, Table 1) show a main strike-slip regime (n = 16) and a less frequent compressive regime (n = 6). There is also a local extension regime (n = 4) at the Archibarca and Culampaja fault systems, here interpreted as local transfer zones along the strike-slip faults.

In the third episode (< 4 Ma), σ_1 orientations show a shift towards NNE-SSW (N20°-30°) with minor scattered data with a N-S orientation (Fig. 8C). The sites of measurement of these stress tensors are mainly located in the volcanic arc axis. The dominant regime is strike-slip at 7 out of 10 reduced stress tensors (Table 1), while the remaining tensors are represented by local pure compression (n = 1) and pure extension (n = 2).

4.3. Miocene-Quaternary magma-feeding fractures

In the study area, we recognized 847 volcanic vents distributed at 130 polygenic and monogenic volcanic centers. For eroded volcanoes, we inferred a vent position in the uppermost part of the edifice. Figure 9 shows the directions of σ_{Hmax} assumed as parallel to the magma-feeding fracture obtained from the edifice elongations and vent alignment. The various σ_{Hmax} have been separated in the same three time periods that were previously recognized by the structural kinematic and dynamic analyses. This allows a direct comparison between volcanic and structural data.

In the first episode (23-8 Ma), σ_{Hmax} axes are distributed in two maxima in correspondence of NW-SE and NE-SW, followed by very few scattered data in other directions. The heterogeneity of σ_{Hmax} distribution is related to the positions of emplacement of volcanic centers; the group with a NW-SE tendency is mainly concentrated in the southern part of the study area (ca. 25'30°S) related to the Culampaja Fault system. The second group of σ_{Hmax} directions (NE-SW) is located in the central and northern part of the study area (Fig. 9A) and is associated with the Aguas Calientes-Guanaqueros faults. Several volcanoes in this episode have geometric relations with the reverse faults active in the same period. For example, in Figure 10A the elongation of Aguas Calientes volcano and the related, parallel alignment of vents (ca. 13 Ma; Villa et al., 2019) suggest a possible NNE-SSW magma-feeding system, parallel to the strike of Aguas Calientes Fault, which was active in the Lower Miocene until ca. 12 Ma. This result is particularly interesting since the regional stress regime in this period was characterised by contraction along an E-W direction, which is unfavorable to magma uprising to the surface. This example is similar to a series of other sites where it is possible to observe the same volcano elongation parallel to the reverse fault strike.

The second episode comprises 82 σ_{Hmax} of volcanoes, active between 8 and 4 Ma. The rose diagram shows a main NW-SE σ_{Hmax} orientation (Fig. 9B), homogeneous in all the study area. There is a second minor peak of NE-SW σ_{Hmax} directions of, which is restricted to the trace of the Arizaro-Pedernales Fault (Naranjo et al., 2018). The morphometric characteristics of volcanoes and vents located above this fault trace indicate a NE-SW magma-feeding fracture, whereas those located on the fault hanging-wall block indicate NW-SE feeding fractures (Fig. 10B).

In the third episode (< 4 Ma), we obtained data at 20 sites with σ_{Hmax} axes scattered between NW-SE, N-S and NE-SW directions (Fig. 9C). Data are mainly concentrated in the central part of the study area (25°S to 15°30'S) and are spatially related to the Lazufre magmatic body (Anderssohn et al., 2009; **Ruch and Walter, 2010**). In general, the deposits associated with this magmatic body correspond to the Pleistocene-Holocene activity of Lastarria and Cordon del Azufre volcanoes. These volcanoes alignment into sector have directions NS in Pleistocene Volcanoes and change principally NW-SE direction in Holocene Volcanoes. These morphometric characteristics, indicating possible magma-feeding fractures with main N-S and NW-SE orientations.

5. Discussion

5.1 Fault and stress evolution in the Western Cordillera

The data collected in this work allow us to recognize three main tectonic stages active from the Miocene to the Quaternary. According to these data, we can propose an evolution model for the Western cordillera between 20°S and 27°S. First, there has been a compressional stage with reverse faulting and a ca. E-W shortening, followed by a left-lateral strike-slip stage, and finally by a right-lateral strike-slip to transpressional phase. The stages recognized in the present work have been integrated and compared with data on the conterminous zones published by Tibaldi et al. (2009), Tibaldi and Bonali (2018) and Giambiagi et al. (2016), to understand the Neogene variation of the stress state in the Western Cordillera and in the western border of the Altiplano-Puna plateau.

Tibaldi et al. (2009) divided the tectonic evolutions of the Western Cordillera north of Salar de Atacama (a in Fig. 1) into four phases. The first, with E-W shortening by reverse faults in the northern part of the area and WNW–ESE shortening in the southern part, was dated to the Miocene. The second and third phases, of Pliocene age, are characterized by a NW-SE horizontal σ_1 and differentiate due to a permutation of σ_v from σ_3 to σ_2. The last phase, dated to the late Pliocene–Quaternary, is characterized by an extensional regime with a NE-SW horizontal σ_3 and a vertical σ_1 (Fig. 11). Giambiagi et al. (2016) studied the stress field variations along the southern part of the Altiplano and North and South of the Puna and reported a first tectonic stage related to the build-up of the Altiplano/Puna Plateau and a second stage characterized by its gravitational collapse. The transition between the two stages is characterized by four stress states, which are: 1) dominant E-W compression, 2) strike-slip with N-S compression and E-W extension, 3) strike-slip regime with E-W compression and N-S extension, and 4) N-S dominant extension stage.

The first stage that has been determined in the present work, with the E-W σ_1, is associated to a permutation of σ_2/σ_3 at ca.12 Ma, which produced a change from a compressional to a strike-slip regime. This E-W compressional phase was recognized in diachronical moments along the Western Cordillera at ca. 20°S from the Middle Miocene to the Upper Miocene, also by Tibaldi et al. (2009). However, in the Paniri area, the E-W compression was recognized as active before the Middle

Miocene (Giambiagi et al., 2016), and at 26.5°S this compressional stage was active at a later stage, since the Upper Miocene (Figure 9).

The E-W compressional stage is comparable with the Quechua Phase recognized in the South of Peru and Central Chile (Mercier et al., 1992; Noblet et al., 1996; Diraison et al., 1998). Similar compressional features, like reverse faults and folds, have been described along the Western Cordillera and Altiplano/Puna Plateau. In the north of Salar de Atacama, the compressional features developed mainly between 35-27 Ma and 19-7 Ma (Noblet et al., 1996; Elger et al., 2005), with local tectonic quiescence and episodic extension at 27-19 Ma (Noblet et al., 1996). After 10 Ma, compressional deformation migrated to the East towards the Sub-Andean region (Allmendinger and Gubbels, 1996; Herail et al., 1996; Kley et al.,1996). Northeast of the Salar de Atacama, at 25-21 Ma, the shortening activity migrated from the Eastern Cordillera to the Sub-Andes ranges (Horton et al., 2018, and references therein). The same temporal events are proposed by Sheuber et al., (2005), who report a compressional phase with uplift of portions of the basement at 33-30 Ma in the Western Cordillera, and shortening in the foreland at 17 Ma.

In the southern part of Western Cordillera, Naranjo et al. (2013a) determined a reverse activity along the Arizaro-Pedernales Fault at 13-14 Ma. In the Puna, the Lower Miocene tectonic activity is characterized by several discrete compressional events with WNW-ESE shortening axis (Marret et al., 1994). The main fault in this area corresponds to the Antofalla System, with reverse activity in the Lower Miocene with E-W to WNW-ESE shortening axes (Kreamer et al., 1999). On the other hand, compressional features were described in the forearc in the north of Chile. The main structure corresponds to a blind reverse fault with long-lived activity from Cretaceous until Upper Miocene (Arriagada et al., 2006; Martinez et al., 2017; Villa et al., 2019), which was active in the western border of the Western Cordillera until the Pleistocene (Gonzalez et al., 2009; Tibaldi et al., 2017).

The second tectonic stage in our work is characterized by a strike-slip regime under a NW-SE to N-S σ_1, active between 8 and 4 Ma. The computation of stress tensors in Western Cordillera reveals that in the north part of study area between 19°S and 23°S the stress field changed first with a rotation of σ_1, from an E-W to a NW-SE position, followed by σ_2 that became horizontal and σ_3 vertical (Box 2, Fig. 11). The differences between the two phases in the northern part of the Western Cordillera is the change in the stress regime from compressional to strike-slip (Tibaldi et al., 2009). In the south part of area, between 24°S to 26°S, the change in the stress tensor was characterized by a clockwise rotation of σ_{Hmax} from an E-W to a NW-SE position in the Lower Miocene, and ca. N-S in Lower Pliocene. At the same time, in the southern part of Central Andes a change in the stress field occurred in the Middle Miocene, while in the south the permutations σ_1/σ_2 and σ_2/σ_3 occurred in the Lower Pliocene (Giambiagi et al., 2016).

The stress field in this stage was related to right-lateral slip along NW-SE faults between 8 to 3 Ma, distributed into three main structures: Calama-Olacapato-El Toro fault (Tibaldi et al., 2009), in the

North of the Puna; Archibarca and Culampaja fault system in the south of Puna sector; Pedernales Incahuasi in the most southern part of the volcanic arc (Giambiagi et al., 2016). The presence of NW-SE faults has been recognized along the southern part of Central Andes (Salfity, 1985) mainly in the backarc, with activity until the Pleistocene (Marret et al., 1994; Salfity, 1985; Viramonte et al., 1984; Riller et al., 2001; Richard and Villanueve, 2002) and in the volcanic arc, which controlled the presence of volcanic centers and collapse caldera evolutions (Riller et al., 2001; Richard and Villanueve, 2002). In the forearc, these fault systems have been active since the Paleocene (Richard et al., 2001) and facilitated the movement and entrapment of magmatic bodies (Yañez and Rivera, 2019). The origin of these NW-SE faults, oblique to the plate margin, has been related to reactivations of inherited discontinuities located in the upper crust (Riller et al., 2001; Schoenbohm and Strecker, 2009; Lanza et al., 2013), or alternatively by “slip partitioning” resulting from oblique plate convergence (Fitch, 1972; Cladouhos et al., 1994).

The third stage recognized in our work in the south segment (24°S to 26°S), is characterised by a stress tensor with σ_1 in an approximate NNE-SSW position under a transtensional regime active after 4 Ma. In the northern part of the volcanic arc, the Pleistocene stress field is characterized by extension with a NE-SW σ_3 (Tibaldi et al., 2009); the same observation was determined in the Paniri region with σ3 with NNE-SSW to NNW-SSE directions (Giambiagi et al., 2016). Between 24°S and 26°S the stress tensors show a clockwise rotation from a ca. N-S to a NE-SW orientation, and a permutation between σ_2/σ_3 in the Pleistocene, which triggers a change in the stress regime from strike-slip to extension (Giambiagi et al., 2016). On the other hand, in the southern part of the Western Cordillera (26.5°S), during the Pleistocene, the regime is strike-slip with a N-S σ_3 and extensional with σ_3 in an E-W position, which represents a permutation of σ_1/σ_2 and σ_2/σ_3 active in the area since the Pleistocene (Giambiagi et al., 2016).

Results presented in our work suggest a transtensional to extensional phase active from the Upper Pliocene to the Pleistocene, active diachronously along the margin of the magmatic arc. In the Altiplano segment (20°S to 23°S), several NW-SE-striking normal faults cut the Pleistocene volcanic deposits (Tibaldi et al., 2006, 2009; Vezzoli et al., 2008). East of the Salar de Atacama, normal faults and extensional fractures with NE-SW to E-W extensional axes affect Pliocene to Pleistocene deposits (Tibaldi et al., 2018). These extensional structures had been interpreted as younger than compressional deformations (Lahsen et al., 1982) or contemporaneous to shortening events (Allmendinger et al., 1986; Tibaldi et al., 2018). Elger et al. (2005) interpreted contemporaneous extensional and contractional faults as local features related to forelimbs collapse.

In the Puna segment between 23°S to 28°S, several extensional structures were reactivated under a WNW-ESE horizontal extension and vertical shortening (Daxberguer and Riller et al., 2015). The change in the stress field was observed in the Antofalla fault, with an ENE-WSW strike-slip fault and a parallel normal fault, interpreted as a gravitational slide (Kreamer et al., 1999). This extensional phase in the Puna sector started after 9 Ma with a N-S σ_3 direction (Lanza et al., 2013).

In conclusion, we found in the study area a Neogene tectonic evolution consistent with previous findings. These events were characterized by a large amount of shortening, concordant with the convergence directions (Pardo Casas and Molnar, 1987), permutations of σ_{Hmax} and clockwise rotations of principal stress axes.

5.2 Possible causes of stress change

As described in the previous section, the identified main tectonic phases are consistent with deformation events described in adjacent areas. The changes of the stress field can be resumed as: (1) Permutation of principal axes, leading to different regimes of contraction, followed by transcurrence, and finally by extension, and (2) clockwise rotation of σ_{Hmax} from E-W to N-S orientation.

Regarding the permutations of principal stress axes, the stress regime varied during Upper Miocene (ca.8 Ma) from pure contractional to transpressional in stage one, to pure transcurrent in stage two. Then in the Upper Pliocene (Ca. 4 Ma) from transtensional to extensional in the third stage. For this reason, σ_1/σ_2 and σ_2/σ_3 stress permutations may be invoked. During the transitions, different and coeval faulting regimes can be active at the same time (Giambiagi et al., 2016).

In the Central Andes, like any continental margin, the regional stress field is responds to transfer of body forces from the Pacific oceanic plate to the South America continental plate (Assumpcao, 1992; Tibaldi et al., 2017), combined with topography-induced forces (Dalmayrac and Molnar, 1981; Froidevaux and Isacks, 1984; Zoback and Magge, 1991; Coblentz and Richardson, 1996) and rheology conditions of lower and upper crust, associated with heat flow (Kusznir, 1991; Richardson and Coblentz, 1994).

We consider that the convergence angle did not change significantly in terms of direction and velocity during the Neogene (Pardo casas and Molnar, 1987; Somoza and Ghidella, 2005, 2012), and that lithospheric vertical stress σ_{zz} increases with thickness and with the low-density anomaly, associated to magma bodies, beneath the mantle. However, in the upper crust σ_{zz} is maintained constant and equal to the lithostatic load (Fleitout and Froidevaux et al., 1982). We propose a model where the permutations of principal stress axes occur as a response to the decrease of horizontal stress σ_{xx} associated with variations of crustal thickness during orogenic construction. In this model, the orogenic growth produced by compression is accommodated by reverse faulting, then, when a certain thickness is reached, the shortening of the crust is absorbed by strike-slip faulting first and then there are extension product of orogenic collapse (Sébrier et al., 1988; Meijer et al., 1997; Giambiagi et al., 2016; Tibaldi et al., 2017). These change in the regimen is produced when a critical thickness point is reached. Thus, if the mean elevation is between 3700 and 4000 m where the tectonic regime preferent is strike-slip, whereas in altitudes higher than 4000 m a.sl, the dominant regime is extensional (Sébrier et al., 1988).

The switch from E-W contraction to strike-slip with N-S extension started in the Middle Miocene in the Puna segment (24 to 26°S) and in the Pliocene in the Altiplano (20°S to 22°S). Our data are concordant with the ages when paleo-elevations reach altitudes higher than 3700 m a.s.l., at ca. 10 Ma in the Puna segment and at ca. 5 Ma BP in the Altiplano (Schildgen and Hoke, 2018, and references therein).

On the other hand, σ_{Hmax} rotations occur diachronously between Upper Miocene and Upper Pliocene. This pattern is characterized by clockwise rotation of σ_1 first from E-W to NW-SE, and then from NNW-SSE to NE-SW. The age of rotations of the stress field is concordant with the change in the relative motion of the South American plate from E-W movement to NE-SW, found between 10 and 3.2 Ma (Pardo-Casas and Molnar, 1987; Marret and Strecker, 2000), consistent with the concept that the movement of the South American plate controls the upper crust deformation (Marret and Strecker, 2000). Other considerations to explain the rotation of the stress field are based on the presence of heritage faults that act to accommodate the differential shortening related to formations of the Bolivian Orocline (Kley et al., 1999; Riller et al., 2001). It is possible, therefore, that interactions of two or more processes controlled the σ_{Hmax} rotations in the volcanic arc during the Neogene.

5.3 Orientations of magma paths

To analyze the evolution of magma paths in the Western Cordillera, south of the Pica Volcanic Gap (Ca.19°S) (Worner et al., 1994), we have integrated the new data obtained in this work with the magma paths reconstructed by Tibaldi et al. (2017). In the northern part of the area, between 19°S and 23°S South of the Altiplano, the magma paths of Tibaldi et al. (2017) for the Miocene were mostly oriented NNE-SSW and subordinately NW-SE (Fig. 12). These orientations are somewhat similar to the magma path orientations obtained for the Lower to Middle Miocene in the present work, which show two main orientations: NE-SW and NW-SE. Since the Pliocene, the magma paths in the North domain (19°S to 23°S) have NNE-SSW to N-S orientations and are concentrated southeast of the Salar de Atacama. In South segment (24°S to 26°S), magma paths have orientation between NW-SE and NE-SW during the Lower and Middle Miocene. Then between Upper Miocene to Lower Pliocene the magma paths have NW-SE direction. Since Upper Pliocene the magma paths are in NNE-SSW to NNW-SSE (Figure 12). These findings are unexpected, because the classical models predict the intrusion of magma along dikes preferentially oriented parallel to the σHmax (Nakamura, 1977; Nakamura et al., 1977). In plate convergence zones, σHmax usually coincides with the convergence direction (Nakamura and Uyeda, 1980). In the central Andes, the convergence of the

Nazca plate was in a WNW direction in the Lower Miocene (Pardo-Casas and Molnar, 1987), and rotated to an E-W position in more recent times (Heidbach et al., 2008).

The NNE-SSW magma paths orientation in the Altiplano area is parallel to sub-parallel to the subduction trench. This can be explained by the presence of a melt zone that forms and rises following the contour of the subduction zone (Tibaldi et al., 2017). However, in the Central Andes, the distribution of volcanoes are mainly controlled by discontinuities in the upper crust (e.g.: Riller et al., 2001; Acocella et al., 2007; Tibaldi et al., 2018; Naranjo et al., 2018b). It is therefore likely that such a connection exists between the orientation of inherited faults and distribution of magma paths. This hypothesis is supported by the presence of faults and folds with N-S to NNE-SSW directions in the Western Cordillera and Sub-Andean Zone (Elger et al., 2005). However, in the Altiplano Plateau there are normal faults with the same orientations (Allmendinger et al., 1997). The fact that these structures are parallel to sub-parallel to magma paths supports the hypothesis that the volcanoes in the Miocene were controlled by the discontinuities in the upper crust. In the case of the normal faults in the Altiplano, the vertical attitude of $\sigma 1$ was favorable to magma uprising. In correspondence of compressional structures instead, with a horizontal $\sigma 1$ perpendicular to magma paths, magma emplacement can be explained by rise in conjugate zones (Naranjo et al., 2018a), large magma overpressure (Gonzalez et al., 2009), rise along reverse fault planes or their splay faults (Galland et al., 2003; Tibaldi, 2008), or local extension within fold hinges (Gürer et al., 2016). A particularly nice example is given by the case portrayed in Figure 10B, where the alignment of vents located above the reverse fault trace indicates a NE-SW magma-feeding fracture, parallel to the fault strike. Instead, another group of vents, located on the fault hanging-wall block, indicate NW-SE magma-feeding fractures. The magma path parallel to the fault strike can be explained by a direct control of the main reverse fault plane, or of a fault splay, consistent with the Tibaldi (2008) model. The NW-SE magma paths can correspond to a local reorientation of the stress tensor in the hanging-wall block at a greater distance from the reverse fault plane.

The NW-SE magma paths observed in the Miocene in the Altiplano segment by Tibaldi et al. (2017) are consistent with the magma paths observed in the Lower Miocene to Lower Pliocene in the Puna segment (Fig. 12). These magma paths are parallel or sub-parallel to several faults found in the study area. In the Altiplano segment, the principal groups of magma path orientations are related to the position and geometry of the Calama-Olacapato-El toro fault system (Salfity, 1985; Riller et al., 2001; Bonali et al., 2012; Lanza et al., 2013). While in the south, the magma path distribution ranges between the Archibarca fault system (Richard and Villanueve, 2002) and the Culampaja fault system (Salfity, 1985).

The age and distribution of volcanic edifices and related magma paths, indicate that in the Puna and Altiplano segments, there was a maximum in volcanic activity since ca. 10 Ma BP. This is consistent with previous authors that showed high magmatic activity in the arc since 10 Ma BP, which decreased at 3 Ma BP (Trumbull et al., 2006; DeCelles et al., 2015). In this period, the fault regime was trascurrent with a NNW-SSE σHmax and dominant NW-SE strike-slip faults. Strike-slip faults, which usually have a vertical attitude, can act as deep weakness zones intercepting magma batches and thus favouring magma upwelling (Tibaldi, 1992). The NW-SE faults found in the Chile volcanic arc, have been, in fact, suggested to control magma upwelling (Riller et al., 2001, 2012; Caffe et al., 2002; Chernicoff et al., 2002; Petrinovic et al., 2005; Ramelow et al., 2006; Trumbull et al., 2006; Bonali et al., 2012; Lanza et al., 2013). Opposite to this situation, in the previous time period (> 8 Ma) when reverse faults and folds were active, in the study area there was less volcanic activity. According to these data, we can infer that the increase in the magmatic volume erupted in the Upper Miocene to Pleistocene is related to a change in the regional stress field that activated NW-SE-striking, high-angle faults, which favoured magma rise from deep sources. A note of caution is due here since other magmatic processes have been described for the same time period to explain the increase in erupted volumes like flare-up magmatism (de Silva, 1989; Worner et al., 2018), variations in the angle of subduction of slab and delamination processes (Kay et al., 1994) and internal control in the development of volcanic arc (DeCelles et al., 2015).

5. Conclusions

The new field study of the Neogene structures in the Western Cordillera between 24°S to 25°S and integration of previous works between ca. 20°S and 26°S allow us to determine three main tectonic events:

(1) A first stage characterized by a compressional regime with E-W σ1 and the presence of reverse faults and folds. In the altiplano domain (19-23°S) this regime was active until the Upper Miocene, while in the south part of (23-26°S) it was active during the Middle Miocene (ca.12 Ma).

(2) A strike-slip stage characterized by NW-SE transpressional to left-lateral faults with NW-SE to NNW-SSE σ1. In the North part of western cordillera and in at 26°S, this stage was active during the Pliocene. Moreover, this stage was active, between 24°S and 26°S, from the Upper Miocene (ca. 8 Ma) to the Pliocene (ca. 4 Ma).

(3) The deformation after 4 Ma was dominated by a right lateral strike-slip passing to extensional regimen, where the σHmax were N-S to NE-SW.

The tectonic stages defined in this work are associated with two dynamic processes: i) The change in the stress field from compressional to strike-slip and strike-slip to extensional is associated to σ1/σ2 and σ2/σ3 permutations and may be explained as resulting from orogen-perpendicular collapse. ii) Rotations of σHmax from E-W to NW-SE position and then NNE-SSW orientation. This shift in the stress field can be associated with the change in the relative South America movements from E-W to NE-SW and reactivations of pre-existing structures with a NW-SE strike.

Our analysis of volcano elongations and vents alignments reveals strong control of NW-SE, N-S and NE-SW faults in the distributions of volcanism in the Western Cordillera. The magma paths with N-S to NE-SW directions are associated with reverse faults active in the Puna domain in the Neogene and normal faults located in the Altiplano domain. The NW-SE magma paths are related to pre-existing NW-SE strike-slip faults.

The increase in volume of volcanism in the southern part of the Central Andes is coeval with the transition from reverse to strike-slip faulting and thus to regional stress field changes.

Acknowledgments

This study was funded by the Agencia Nacional de Investigación y Desarrollo (ANID) –PFCHA (Programa Formación de Capital Humano Avanzado) Doctorado Nacional 2019-21191039. The authors want to thank project CRC 1211 “Earth-Evolution at the dry limits”, specially to Dr. Eduardo Campos, for providing support to field work.

References

Acocella, V., Vezzoli, L., Omarini, R., Matteini, M., & Mazzuoli, R. (2007). Kinematic variations across Eastern Cordillera at 24 S (Central Andes): tectonic and magmatic implications. Tectonophysics, 434(1-4), 81-92.

Allmendinger, R. W., Cardozo, N., & Fisher, D. M. (2011). Structural geology algorithms: Vectors and tensors. Cambridge University Press.

Allmendinger, R.W., Gubbels, T., (1996). Pure and simple shear plateau uplift, Altiplano–Puna, Argentina and Bolivia. Tectonophysics 259, 1–13.

Allmendinger, R.W., (1986). Tectonic development, southeastern border of the Puna Plateau, northwestern Argentine Andes. Geol. Soc. Am. Bull. 97:1070–1082. http://dx.doi.org/10.1130/0016-7606(1986).

Allmendinger, R.W., Strecker, M., Eremchuk, E., Francis, P., (1989). Neotectonic deformation of the southern Puna Plateau, northwestern Argentina. J. S. Am. Earth Sci. 2 (2), 111–130.

Allmendinger, R.W., Jordan, T.E., Kay, S.M., Isacks, B.L., (1997). The evolution of the Altiplano - Puna Plateau of the central Andes. Annu. Rev. Earth Planet. Sci. 25, 139–174.

Allmendinger, R.W., (2018). FaultKinWin Full version 8.0.7. A program for analyzing fault slip data for windows system. Retrieved from. www.geo.cornell.edu/geology/faculty/RWA/programs.html.

Angelier, J. (1990). Inversion of field data in fault tectonics to obtain the regional stress—III. A new rapid direct inversion method by analytical means. Geophysical Journal International, 103(2), 363-376.

Anderson, E.M., (1951). The Dynamics of Faulting and Dyke Formation with Applications to Britain. Oliver and Boyd, White Plains, New York.

Arriagada, C., Cobbold, P. R., & Roperch, P. (2006). Salar de Atacama basin: A record of compressional tectonics in the central Andes since the mid-Cretaceous. Tectonics, 25(1).

Assumpcao, M. (1992). The regional intraplate stress field in South America. Journal of Geophysical Research: Solid Earth, 97(B8), 11889-11903.

Aydin, A., & Schultz, R. A. (1990). Effect of mechanical interaction on the development of strike-slip faults with echelon patterns. Journal of Structural Geology, 12(1), 123-129.

Baby, P., Moretti, I., Guillier, B., Limachi, R., Mendez, E., Oller, J., Specht, M., (1995). Petroleum system of the northern and central Bolivian sub-Andean zone. In: Petroleum Basins of South America, AAPG Special Volumes Vol. M 62. pp. 61–82.

Barrionuevo, M., Giambiagi, L., Mescua, J. F., Suriano, J., De la Cal, H., Soto, J. L., & Lossada, A. C. (2019). Miocene deformation in the orogenic front of the Malargüe fold-and-thrust belt (35 30′–36 S): Controls on the migration of magmatic and hydrocarbon fluids. Tectonophysics, 766, 480-499.

Barton, C. A., & Zoback, M. D. (1994). Stress perturbations associated with active faults penetrated by boreholes: Possible evidence for near-complete stress drop and a new technique for stress magnitude measurement. Journal of Geophysical Research: Solid Earth, 99(B5), 9373-9390.

Bascuñán, S., Arriagada, C., Le Roux, J., Deckart, K., (2015). Unraveling the Peruvian phase of the Central Andes: stratigraphy, sedimentology and geochronology of the Salar de Atacama Basin (22°30–23°S), northern Chile. Basin Res. 28, 365–392.

Beck, S.L., Zandt, G., (2002). The nature of orogenic crust in the central Andes. J. Geophys. Res. 107 (B10), 2230.

Bonali, F., Corazzato, C., Tibaldi, A., (2011). Identifying rift zones on volcanoes: an example from La Réunion Island, Indian Ocean. Bull. Volcanol. 73, 347–366. http://dx.doi.org/10.1007/s00445-010-0416-1.

Bonali, F. L., Corazzato, C., & Tibaldi, A. (2012). Elastic stress interaction between faulting and volcanism in the Olacapato–San Antonio de Los Cobres area (Puna plateau, Argentina). Global and planetary change, 90, 104-120.

Caffe, P.J., Trumbull, R.B., Coira, B.L., Romer, R.L., (2002). Petrogenesis of early volcanic phases in Northern Puna Cenozoic magmatism. Implications for magma genesis and crustal processes in the Central Andean Plateau. J. Petrol. 43, 907–942.

Chernicoff, C.J., Richards, J.P., Zappettini, E.O., (2002). Crustal lineament control on magmatism and mineralization in northwestern Argentina: geological, geophysical and remote sensing evidence. Ore Geol. Rev. 21, 127–155.

Carrapa, B., Adelmann, D., Hilley, G.E., Mortimer, E., Sobel, E.R., Strecker,M.R., (2005). Oligocene range uplift and development of plateau morphology in the southern central Andes. Tectonics 24, TC4011.

Cas, R.A.F., Wright, J.V., (1987). Volcanic Successions. Allen & Unwin, London (528 pp).

Charrier, R., Pinto, L., Rodríguez, M.P., (2007). Tectonostratigraphic evolution of the Andean orogen in Chile. In: Moreno, T., Gibbons, W. (Eds.), The Geology of Chile. The Geological Society, London, pp. 21–114.

Chaussard, E., Amelung, F., (2014). Regional controls on magma ascent and storage in volcanic arcs. Geochem. Geophys. Geosyst. 15, 1407–1418. http://dx.doi.org/10.1002/2013GC005216.

Chiba, T., Kaneta, S. I., & Suzuki, Y. (2008). Red relief image map: new visualization method for three-dimensional data. The international archives of the photogrammetry, remote sensing and spatial information sciences, 37(B2), 1071-1076.

Cladouhos, T.T., Allmendinger, R.W., Coira, B., Farrar, E., (1994). Late Cenozoic deformation in the Central Andes: fault kinematics from the northern Puna, northwestern Argentina and southwestern Bolivia. J. S. Am. Earth Sci. 7 (2), 209–228.

Coblentz, D. D., & Richardson, R. M. (1996). Analysis of the South American intraplate stress field. Journal of Geophysical Research: Solid Earth, 101(B4), 8643-8657.

Corazzato, C., Tibaldi, A., (2006). Basement fracture control on type, distribution, and morphology of parasitic volcanic cones: an example from Mt. Etna, Italy. In: Tibaldi, A., Lagmay, M. (Eds.), Interaction between Volcanoes and their Basement. J. Volcanol. Geotherm. Res., Vol. 158, pp. 177–194.

Coutand, I., Cobbold, P.R., de Urreiztieta, M., Gautier, P., Chauvin, A., Gapais, D., Rossello, E.A., Lopez-Gamundì, O., (2001). Style and history of Andean deformation, Puna plateau, northwestern Argentina. Tectonics 20, 210–234.

Cornejo, P.; Mpodozis, C. (1996). Geología de la Región de Sierra Exploradora (25°-26° Lat. S). Servicio Nacional de Geología y Minería, Informe Registrado IR-96-09, 2 Vols. Santiago.

Dalmayrac, B., & Molnar, P. (1981). Parallel thrust and normal faulting in Peru and constraints on the state of stress. Earth and Planetary Science Letters, 55(3), 473-481.

Daxberger, H., & Riller, U. (2015). Kinematics of Neogene to Recent upper-crustal deformation in the southern Central Andes (23–28 S) inferred from fault–slip analysis: evidence for gravitational spreading of the Puna Plateau. Tectonophysics, 642, 16-28.

DeCelles, P.G., Horton, B.K., (2003). Early to middle Tertiary foreland basin development and the history of Andean crustal shortening in Bolivia. Geol. Soc. Am. Bull. 115, 58–77.

DeCelles, P. G., Zandt, G., Beck, S. L., Currie, C. A., Ducea, M. N., Kapp, P., ... & Schoenbohm, L. M. (2014). Cyclical orogenic processes in the Cenozoic central Andes. Geological Society of America Memoirs, 212, MWR212-22.

Deeken, A., Sobel, E.R., Coutand, I., Haschke, M., Riller, U., Strecker, M.R., (2006). Development of the southern Eastern Cordillera, NW Argentina, constrained by apatite fission track thermochronology: from early Cretaceous extension to middle Miocene shortening. Tectonics 25 (6).

de Silva, S.L., (1989). Altiplano-Puna volcanic complex of the Central Andes. Geology 17, 1102–1106.

del Rey, A., Deckart, K., Arriagada, C., Martínez, F., (2016). Resolving the paradigm of the late Paleozoic–Triassic Chilean magmatism: Isotopic approach. Gondwana Res. 37, 172–181.

Delvaux, D., Moeys, R., Stapel, G., Petit, C., Levi, K., Miroshnichenko, A., ... & San'kov, V. (1997). Paleostress reconstructions and geodynamics of the Baikal region, central Asia, Part 2. Cenozoic rifting. Tectonophysics, 282(1-4), 1-38.

Diraison, M., Cobbold, P., Rossello, E., Amos, A., (1998). Neogene dextral transpression due to oblique convergence across the Andes of northwestern Patagonia, Argentina. J. South Am. Earth Sci. 11, 519–532.

Dupin, J. M., Sassi, W., & Angelier, J. (1993). Homogeneous stress hypothesis and actual fault slip: a distinct element analysis. Journal of Structural Geology, 15(8), 1033-1043.

Echavarria, L., Hernndez, R., Allmendinger, R., Reynolds, J., (2003). Subandean thrust and fold belt of northwestern Argentina: geometry and timing of the Andean evolution. AAPG Bull. 87 (6), 965–985.

Eichelberger, N., McQuarrie, N., Ryan, J., Karimi, B., Beck, S., Zandt, G., (2015). Evolution of crustal thickening in the central Andes, Bolivia. Earth Planet. Sci. Lett. 426, 191–203.

Elger, K., Oncken, O., Glodny, J., (2005). Plateau-style accumulation of deformation: Southern Altiplano. Tectonics 24, TC4020. doi:10.1029/2004TC001675.

Fitch, T.J., (1972). Plate convergence, transcurrent faults, and internal deformation adjacent to Southeast Asia and the Western Pacific. Journal of Geophysical Research 77, 4432–4435.

Fleitout, L., & Froidevaux, C. (1982). Tectonics and topography for a lithosphere containing density heterogeneities. Tectonics, 1(1), 21-56.

Froidevaux, C., & Isacks, B. L. (1984). The mechanical state of the lithosphere in the Altiplano-Puna segment of the Andes. Earth and Planetary Science Letters, 71(2), 305-314.

Galland, O., De Bremond d'Ars, J., Cobbold, P. R., & Hallot, E. (2003). Physical models of magmatic intrusion during thrusting. Terra Nova, 15(6), 405-409.

Galland, O., Cobbold, P.R., de Bremond d'Ars, J., Hallot, E., (2007a). Rise and emplacement of magma during horizontal shortening of the brittle crust: insights from experimental modelling. J. Geophys. Res. http://dx.doi.org/10.1029/2006JB004604.

Galland, O., Hallot, E., Cobbold, P.R., Ruffet, G., and de Bremond d’Ars, J., (2007b), volcanism in a compressional Andean setting: A structural and geochronological study of Tromen volcano (Neuquén Province, Argentina): Tectonics, v. 26, TC4010, doi: 10.1029/2006TC002011.

Gapais, D., Cobbold, P. R., Bourgeois, O., Rouby, D., & de Urreiztieta, M. (2000). Tectonic significance of fault-slip data. Journal of Structural Geology, 22(7), 881-888.

Gardeweg, M., Carlos. F.. Ramírez R., & J.. Davidson M. (1993). Mapa geológico del área del Salar de Punta Negra y del Volcán Llullaillaco, Región de Antofagasta. Servicio Nacional de Geología y Minería.

Garzione, C.N., Hoke, G.D., Libarkin, J.C., Withers, S., MacFadden, B.J., Eiler, J.M., Ghosh, P., Mulch, A., (2008). Rise of the Andes. Science 320, 1304–1307.

Garzione, C.N., Molnar, P., Libarkin, J.C., MacFadden, B.J., (2006). Rapid late Miocene rise of the Bolivian Altiplano: evidence for removal of mantle lithosphere. Earth Planet. Sci. Lett. 241 (3), 543–556.

Germa, A., Connor, L.J., Cañon-Tapia, E., Le Corvec, N., (2013). Tectonic and magmatic controls on the location of post-subduction monogenetic volcanoes in Baja California, Mexico, revealed through spatial analysis of eruptive vents. Bull. Volcanol. 75 (12), 1–14.

Giambiagi, L., Alvarez, P., Spagnotto, S., (2016). Temporal variation of the stress field during the construction of the central Andes: constrains from the volcanic arc region (22–26° S), Western Cordillera, Chile, during the last 20 Ma. Tectonics 35 (9), 2014–2033.

Ghosh, P., Garzione, C.N., Eiler, J.M., (2006). Rapid uplift of the Altiplano revealed through 13C–18O bonds in paleosol carbonates. Science 311, 511–515.

Glazner, A.F., (1991). Plutonism, oblique subduction, and continental growth: an example from the Mesozoic of California. Geology 19, 784–786.

Grosse, P., Guzmán, S., & Petrinovic, I. (2017). Volcanes compuestos cenozoicos del noroeste argentino. Ciencias de la Tierra y Recursos Naturales del NOA. Relatorio del XX Congreso Geológico Argentino, Tucumán, Argentina.

González, G., Cembrano, J., Aron, F., Veloso, E. E., & Shyu, J. B. H. (2009). Coeval compressional deformation and volcanism in the central Andes, case studies from northern Chile (23 S–24 S). Tectonics, 28(6).

Gonzalez, R., Wilke, G.H., Menzies, A.H., Riquelme, R., Herrera, C., Matthews, S., Espinoza, F., Cornejo, P., (2015). Carta Sierra de Varas, Región de Antofagasta. Servicio Nacional de Geología y Minería, Carta Geológica de Chile. Serie Geología Básica 178, 1 mapa escala 1:100.000.

Gubbels, T.L., Isacks, B.L., Farrar, E., (1993). High-level surfaces, plateau uplift and foreland development, Bolivian central Andes. Geology 2 (1), 695–698.

Gudmundsson, A., (2006). How local stresses control magma-chamber ruptures, dyke injections, and eruptions in composite volcanoes. Earth Sci. Rev. 79, 1–31.

Gudmundsson, A., (2012). Magma chambers: formation, local stresses, excess pressures, and compartments. J. Volcanol. Geotherm. Res. 237–238, 19–41.

Gürer, D., Galland, O., Corfu, F., Leanza, H. A., & Sassier, C. (2016). Structure and evolution of volcanic plumbing systems in fold-and-thrust belts: A case study of the Cerro Negro de Tricao Malal, Neuquén Province, Argentina. GSA Bulletin, 128(1-2), 315-331.

Hamilton, W.B., (1995). Subduction systems and magmatism. In: Smellie, J.R. (Ed.), Volcanism Associated with Extension to Consuming Plate Margins. Geol. Soc. London Spec. Publ, Vol. 81, pp. 3–28.

Heidbacha, O., Tingayd, M., Bartha, A., Reineckere, J., Kurfeßa, D., & Müllera, B. (2010). Global crustal stress pattern based on the World Stress Map database release 2008. Tectonophysics, 482, 3-15.

Herail, G., Oller, J., Baby, P., Bonhomme, M., Soler, P., (1996). Strike-slip faulting, thrusting and related basins in the Cenozoic evolution of the southern branch of the Bolivian Orocline. Tectonophysics 259, 201–212.

Hernando, I.R., Franzese, J.R., Llambías, E.J., Petrinovic, I.A., (2014). Vent distribution in the Quaternary Payún Matrú Volcanic Field, western Argentina: its relation to tectonics and crustal structures. Tectonophysics 622, 122–134.

Horton, B. K. (2018). Sedimentary record of Andean mountain building. Earth-Science Reviews, 178, 279-309.

Isacks, B.L., (1988). Uplift of the Central Andean Plateau and bending of the Bolivian orocline. J. Geophys. Res. 93, 3211–3231.

Johnson, A.M., (1970). Physical Processes in Geology: San Francisco, California, Freeman, Cooper & Company, 592 p.

Jordan, T.E., Alonso, R.N., (1987). Cenozoic stratigraphy and basin tectonics of the Andes Mountains, 20°–28° south latitude. AAPG Bull. 71, 49–64.

Kaven, J. O., Maerten, F., & Pollard, D. D. (2011). Mechanical analysis of fault slip data: Implications for paleostress analysis. Journal of structural geology, 33(2), 78-91.

Kay, S.M., Coira, B.L., (2009). Shallowing and steepening subduction zones, continental lithospheric loss, magmatism, and crustal flow under the Central Andean Altiplano-Puna Plateau. In: Kay, S.M., Ramos, V.A., Dickinson, W.R. (Eds.), Backbone of the Americas: Shallow Subduction, Plateau Uplift, and Ridge and Terrane Collision. Geological Society of America Memoir, 204, 229–259.

Kay, S.M., Coira, B., Viramonte, J., (1994). Young mafic back arc volcanic rocks as indicators of continental lithospheric delamination beneath the Argentine Puna plateau, central Andes. J. Geophys. Res. Solid Earth 99 (B12), 24323–24339.

Kervyn, M., Ernst, G.G.J., Carracedo, J.C., Jacobs, P., (2012). Geomorphometric variability of “monogenetic” volcanic cones: evidence from Mauna Kea, Lanzarote and experimental cones. Geomorphology 136 (1), 59–75.

Kley, J., (1996). Transition from basement-involved to thin-skinned thrusting in the Cordillera Oriental of southern Bolivia. Tectonics 15, 763–775.

Kley, J., Monaldi, C.R., (1998). Tectonic shortening and crustal thickness in the Central Andes: how good is the correlation? Geology 26, 723–726.

Kley, J., (1999). Geologic and geometric constraints on a kinematic model of the Bolivian orocline. J. South Am. Earth Sci. 12, 221–235.

Kraemer, B., Adelmann, D., Alten, M., Schnurr, W., Erpenstein, K., Kiefer, E., van den Bogaard, P., Gorler, K., (1999). Incorporation of the Paleogene foreland into the Neogene Puna plateau: the Salar de Antofalla area, NW Argentina. J. South Am. Earth Sci. 12, 157–182.

Kruger, T., & Kisters, A. (2016). Magma accumulation and segregation during regional-scale folding: The Holland's dome granite injection complex, Damara belt, Namibia. Journal of Structural Geology, 89, 1-18.

Kusznir, N. (1991), The distribution of stress with depth in the lithosphere: Thermo-rheological and geodynamic constraints, in Tectonic Stress in the Lithosphere, edited by R. B. Whitmarsh et al., pp. 95–110, R. Soc., London.

Lacombe, O. (2012). Do fault slip data inversions actually yield "paleostresses" that can be compared with contemporary stresses? A critical discussion. Comptes Rendus Geoscience, 344(3-4), 159-173.

Lahsen, A., (1982). Upper Cenozoic volcanism and tectonism in the Andes of northern Chile. Earth Sci. Rev. 18 (3), 285–302.

Lanza, F., Tibaldi, A., Bonali, F. L., & Corazzato, C. (2013). Space–time variations of stresses in the Miocene–Quaternary along the Calama–Olacapato–El Toro fault zone, Central Andes. Tectonophysics, 593, 33-56.

Llambías, E.J., Leanza, H.A., and Galland, O., (2011). Agrupamiento volcánico Tromen-Tilhue, in Leanza, H.A., Arregui, C., Carbone, O., Danieli, J.C., and Vallés, J.M., eds., Geologia y Recursos Naturales de la Provincia del Neuquén, XVIII Congreso Geologico Argentino, Relatorio: Neuquén, Argentina, Asociación Geológica Argentina, p. 627–636.

Lopez, C., Martinez, F., Maksymowicz, A., Giambiagi, L., & Riquelme, R. (2019). What is the structure of the forearc region in the Central Andes of northern Chile? An approach from field data and 2-D reflection seismic data. Tectonophysics, 769, 228187.

Maerten, L. (2000). Variation in slip on intersecting normal faults: Implications for paleostress inversion. Journal of Geophysical Research: Solid Earth, 105(B11), 25553-25565.

Marrett, R., & Allmendinger, R. W. (1990). Kinematic analysis of fault-slip data. Journal of structural geology, 12(8), 973-986.

Marrett, R.A., Allmendinger, R.W., Alonso, R.N., Drake, R.E., (1994). Late Cenozoic tectonic evolution of the Puna plateau and adjacent foreland, northwestern Argentine Andes. J. South Am. Earth Sci. 7, 179–207.

Marrett, R., & Strecker, M. R. (2000). Response of intracontinental deformation in the central Andes to late Cenozoic reorganization of South American Plate motions. Tectonics, 19(3), 452-467.

Martínez, F., Gonzalez, R., Bascuñan, S., & Arriagada, C. (2017). Structural styles of the salar de Punta Negra basin in the preandean depression (24°-25° S) of the central Andes. Journal of South American Earth Sciences, 87, 188-199.

Martınez-Dıaz, J. J. (2002). Stress field variation related to fault interaction in a reverse oblique-slip fault: the Alhama de Murcia fault, Betic Cordillera, Spain. Tectonophysics, 356(4), 291-305.

McQuarrie, N., (2002). The kinematic history of the central Andean fold-thrust belt, Bolivia; implications for building a high plateau. Geol. Soc. Am. Bull. 114, 950–963.

McQuarrie, N., Horton, B.K., Zandt, G., Beck, S., DeCelles, P.G., (2005). Lithospheric evolution of the Andean fold–thrust belt, Bolivia, and the origin of the central Andean plateau. Tectonophysics 399 (1), 15–37.

Meijer, P.Th., Govers, R., Wortel, M.J.R., (1997). Forces controlling the present-day state of stress in the Andes. Earth Planet. Sc. Lett. 148, 157–170.

Mercier, J. L., Sebrier, M., Lavenu, A., Cabrera, J., Bellier, O., Dumont, J. F., & Machrare, J. (1992). Changes in the tectonic regime above a subduction zone of Andean type: The Andes of Peru and Bolivia during the Pliocene-Pleistocene. Journal of Geophysical Research: Solid Earth, 97(B8), 11945-11982.

Moretti, I., Baby, P., Mendez, E., Zubieta, D., (1996). Hydrocarbon generation in relation to thrusting in the Sub Andean zone from 18 to 22 degrees S, Bolivia. Pet. Geosci. 2 (1), 17–28.

Mostafa, M. E. (2005). Iterative direct inversion: An exact complementary solution for inverting fault-slip data to obtain palaeostresses. Computers & geosciences, 31(8), 1059-1070.

Mpodozis, C., Arriagada, C., Basso, M., Roperch, P., Cobbold, P., Reich, M., (2005). Late Mesozoic to Paleogene stratigraphy of the Salar the Atacama Basin, Antofagasta, Northern Chile: implications for the tectonic evolution of the Central Andes. Pag.125–154, Tectonophysics 399.

Mpodozis, C., Ramos, V.A., (2008). Tectónica jurásica en Argentina y Chile: Extensión, Subducción Oblicua, Rifting, Deriva y Colisiones? Rev. Geol. Argent. 63, 479–495.

Nakamura, K., (1977). Volcanoes as possible indicators of tectonic stress orientation-Principle and proposal: Journal of Volcanology and Geothermal Research, v. 2, p. 1–16, doi: 10.1016/0377-0273(77)90012 -9.

Nakamura, K., Jacob, K.H., Davies, J.N., (1977). Volcanoes as possible indicators of tectonic stress orientation – Aleutinian and Alaska. Pure Appl. Geophys., 115, 87–112.

Nakamura, K., Uyeda, S., (1980). Stress gradient in arc-back arc regions and plate subduction. J. Geophys. Res., 85, 6419–6428.

Naranjo, J.A., & Cornejo, P., (1992), Hoja Salar de la Isla: Servicio Nacional de Geología y Minería (Chile) Carta Geológica de Chile 72, scale 1:250,000, 1 sheet.

Naranjo, J.A., Villa, V., and Venegas, C., (2013a). Geología de las áreas Salar de Aguilar y Portezuelo del León Muerto, Regiones de Antofagasta y Atacama: Servicio Nacional de Geología y Minería (Chile) Carta Geológica de Chile, Serie Geología Básica 151 and 152, scale 1:100,000, 1 sheet.

Naranjo, J.A., Villa, V., and Venegas, C., (2013b). Geología de las áreas Salar de Pajonales y Cerro Moño, Regiones de Antofagasta y Atacama: Servicio Nacional de Geología y Minería (Chile) Carta Geológica de Chile, Serie Geología Básica 153 and 154, scale 1:100,000, 1 sheet.

Naranjo, J. A., Hevia, F., Villa, V., & Ramírez, C. A. (2018a). Miocene to Holocene geological evolution of the Lazufre segment in the Andean volcanic arc. Geosphere, 15(1), 47-59.

Naranjo, J. A., Villa, V., Ramírez, C., & Pérez de Arce, C. (2018b). Volcanism and tectonism in the southern Central Andes: Tempo, styles, and relationships. Geosphere, 14(2), 626-641.

Nieto-Samaniego, Á. F. (1999). Stress, strain and fault patterns. Journal of Structural Geology, 21(8-9), 1065-1070.

Noblet, C., Lavenu, A., & Marocco, R. (1996). Concept of continuum as opposed to periodic tectonism in the Andes. Tectonophysics, 255(1-2), 65-78.

Odé, H., (1957). Mechanical analysis of the dike pattern of the Spanish Peaks area, Colorado: Geological Society of America Bulletin, v. 68, p. 567–576, doi: 10.1130/0016-7606 (1957)68 [567:MAOTDP]2.0.CO;2

Pardo-Casas, F., Molnar, P., (1987). Relative motion of the Nazca (Farallon) and South American plates since late Cretaceous time. Tectonics 6, 233–248.

Pasquarè F.A., Tibaldi A. (2003). Do transcurrent faults guide volcano growth? The case of NW Bicol Volcanic Arc, Luzon, Philippines. Terra Nova, 15, 3, 204-212.

Pasquaré G., Tibaldi A., Attolini C., Cecconi G. (1988). Morphometry, spatial distribution and tectonic control of Quaternary volcanoes in northern Michoacan, Mexico. Rend. Soc. Ital. Mineral. Petrol., 43(4), 1215–1225.

Paulsen, T. S., and Wilson, T. J., (2010). New criteria for systematic mapping and reliability assessment of monogenetic volcanic vent alignments and elongate volcanic vents for crustal stress analyses. Tectonophysics, 482(1), 16-28.

Petit, J. P. (1987). Criteria for the sense of movement on fault surfaces in brittle rocks. Journal of structural Geology, 9(5-6), 597-608.

Petrinovic, I.A., Riller, U., Brod, A., (2005). The Negra Muerta volcanic complex, southern Central Andes: geochemical characteristics and magmatic evolution of an episodic volcanic centre. J. Volcanol. Geotherm. Res. 140 (4), 295–320.

Pollard, D. D., & Segall, P. (1987). Theoretical displacements and stresses near fractures in rock: with applications to faults, joints, veins, dikes, and solution surfaces. In Fracture mechanics of rock (pp. 277-347).

Ramos, V.A., (2009). Anatomy and global context of the Andes: main geologic features and the Andean orogenic cycle. In: Kay, S.M., Ramos, V.A., Dickinson,W. (Eds.), Backbone of the Americas: Shallow Subduction, Plateau Uplift, and Ridge and Terrane Collision. Geological Society of América, Memoir vol. 204, pp. 31–65.

Ramelow, J., Riller, U., Romer, R.L., Oncken, O., (2006). Kinematic link between episodic caldera collapse of the Negra Muerta collapse caldera and motion on the Olacapato–El Toro fault zone, NW-Argentina. Int. J. Earth Sci. 95, 529–541. http://dx.doi.org/10.1007/s00531-005-0042-x.

Richards, J. P., & Villeneuve, M. (2002). Characteristics of late Cenozoic volcanism along the Archibarca lineament from Cerro Llullaillaco to Corrida de Cori, northwest Argentina. Journal of Volcanology and Geothermal Research, 116(3-4), 161-200.

Richards, J. P., Boyce, A. J., & Pringle, M. S. (2001). Geologic evolution of the Escondida area, northern Chile: A model for spatial and temporal localization of porphyry Cu mineralization. Economic Geology, 96(2), 271-305.

Richardson, R. M., & Coblentz, D. D. (1994). Stress modeling in the Andes: Constraints on the South American intraplate stress magnitudes. Journal of Geophysical Research: Solid Earth, 99(B11), 22015-22025.

Riller, U., Petrinovic, I., Ramelow, J., Strecker, M., & Oncken, O. (2001). Late Cenozoic tectonism, collapse caldera and plateau formation in the central Andes. Earth and Planetary Science Letters, 188(3-4), 299-311.

Riller, U., Cruden, A. R., Boutelier, D., & Schrank, C. E. (2012). The causes of sinuous crustal-scale deformation patterns in hot orogens: Evidence from scaled analogue experiments and the southern Central Andes. Journal of Structural Geology, 37, 65-74.

Salfity, J. A. (1985). Lineamentos transversales al rumbo andino en el Noroeste Argentino. In IV Congreso Geologico Chileno, (Vol. 2, pp. 119-137), Antofagasta, Chile.

Sasvári, Á., & Baharev, A. (2014). SG2PS (structural geology to postscript converter)–A graphical solution for brittle structural data evaluation and paleostress calculation. Computers & Geosciences, 66, 81-93.

Scheuber, E., Mertmann, D., Ege, H., Silva-Gonzalez, P., Heubeck, C., Reutter, K.-J., Jacobshagen, V., (2005). Exhumation and basin development related to formation of the central Andean plateau, 21°S. In: Oncken (Ed.), The Andes from Top to Bottom. Frontiers in Earth Sciences, p. 1.

Schildgen, T. F., & Hoke, G. D. (2018). The topographic evolution of the central Andes. Elements: An International Magazine of Mineralogy, Geochemistry, and Petrology, 14(4), 231-236.

Schoenbohm, L.M., Strecker, M.R., 2009. Normal faulting along the southern margin of the Puna Plateau, northwest Argentina. Tectonics 28 (5).

Schnurr, W.B.W., Trumbull, R.B., Clavero, J., Hahne, K., Siebel, W., and Gardeweg, M., (2007). Twenty-five million years of silicic volcanism in the southern central volcanic zone of the Andes: Geochemistry and magma genesis of ignimbrites from 25 to 27 °S, 67 to 72 °W: Journal of Volcanology and Geothermal Research, v. 166, p. 17–46, https://doi.org/10.1016/j.jvolgeores.2007.06.005.

Sébrier, M., Lavenu, A., Fornari, M., & Soulas, J. P. (1988). Tectonics and uplift in Central Andes (Peru, Bolivia and northern Chile) from Eocene to present. Géodynamique, 3(1-2), 85-106.

Settle M. (1979). The structure and emplacement of cinder cone fields. Am. J. Science, 279, 1089–1107.

Solari M., Venegas C., Montecino D., Astudillo N., Cortés J., Bahamondes B., Araya C., Espinoza F. (2017). Geología del área Imilac-Quebrada Guanaqueros, Región de Antofagasta. Servicio Nacional de Geología y Minería, Carta Geológica de Chile, Serie Geología Básica 191: 88 p., 1 map at scale 1:100,000. Santiago, Chile.

Somoza, R., & Ghidella, M. E. (2005). Convergencia en el margen occidental de América del Sur durante el Cenozoico: subducción de las placas de Nazca, Farallón y Aluk. Revista de la Asociación Geológica Argentina, 60(4), 797-809.

Somoza, R., & Ghidella, M. E. (2012). Late Cretaceous to recent plate motions in western South America revisited. Earth and Planetary Science Letters, 331, 152-163.

Strecker, M.R., Alonso, R.N., Bookhagen, B., Carrapa, B., Hilley, G.E., Sobel, E.R., Trauth, M.H., (2007). Tectonics and climate of the southern central Andes. Annu. Rev. Earth Planet. Sci. 35, 747–787

Tadini, A., Bonali, F.L., Corazzato, C., Cortés, J.A., Tibaldi, A., Valentine, G.A., (2014). Spatial distribution and structural analysis of vents in the Lunar Crater Volcanic Field (Nevada, USA). Bull. Volcanol. 76 (11), 1–15.

Tibaldi A., (1992). The role of transcurrent intra-arc tectonics in the configuration of a volcanic arc. Terra Nova, 4, 5, 567-577.

Tibaldi, A., (1995). Morphology of pyroclastic cones and tectonics. J. Geophys. Res. 100 (B12), 24,521–24,535.

Tibaldi, A., Bistacchi, A., Pasquaré, F.A., Vezzoli, L., (2006). Extensional tectonics and volcano lateral collapses: insights from Ollague volcano (Chile–Bolivia) and analogue modelling. Terra Nova 18, 282–289. doi:10.1111/j.1365-3121.2006.00691.x.

Tibaldi, A., (2008). Contractional tectonics and magma paths in volcanoes. J. Volcanol. Geotherm. Res. 176: 291–301. http://dx.doi.org/10.1016/j.jvolgeores.2008.04.008.

Tibaldi, A., Corazzato, C., Rovida, A., (2009). Miocene–quaternary structural evolution of the Uyuni–Atacama region, Andes of Chile and Bolivia. Tectonophysics 471 (1), 114–135.

Tibaldi, A., (2015). Structure of volcano plumbing systems: a review of multi-parametric effects. J. Volcanol. Geotherm. Res. 298, 85–135.

Tibaldi, A., & Bonali, F. L. (2017). Intra-arc and back-arc volcano-tectonics: Magma pathways at Holocene Alaska-Aleutian volcanoes. Earth-Science Reviews, 167, 1-26.

Tibaldi, A., Bonali, F. L., & Corazzato, C. (2017). Structural control on volcanoes and magma paths from local- to orogen-scale: The central Andes case. Tectonophysics, 699, 16-41.

Tibaldi, A., & Bonali, F. L. (2018). Contemporary recent extension and compression in the central Andes. Journal of Structural Geology, 107, 73-92.

Tibaldi A., Civelli G., Pecchio M., (1989). Tectonic control on morphometry of cinder cones in Lanzarote and Fuerteventura, Canary Islands. Proceedings of the International Meeting on Canarian Volcanism, Lanzarote, Canary Islands. European Science Foundation, 216–219.

Tibaldi, A., Corazzato, C., & Rovida, A. (2009). Miocene–Quaternary structural evolution of the Uyuni–Atacama region, Andes of Chile and Bolivia. Tectonophysics, 471(1-2), 114-135.

Trumbull, R.B., Riller, U., Oncken, O., Scheuber, E., Munier, K., Hongn, F., (2006). The time-space distribution of Cenozoic volcanism in the South-Central Andes: a new data compilation and some tectonic implications. The Andes. Springer, Berlin Heidelberg, pp. 29–43.

Trumbull, R. B., Wittenbrink, R., Hahne, K., Emmermann, R., Büsch, W., Gerstenberger, H., & Siebel, W. (1999). Evidence for Late Miocene to Recent contamination of arc andesites by crustal melts in the Chilean Andes (25–26 S) and its geodynamic implications. Journal of South American Earth Sciences, 12(2), 135-155.

Twiss, R. J., & Unruh, J. R. (1998). Analysis of fault slip inversions: Do they constrain stress or strain rate?. Journal of Geophysical Research: Solid Earth, 103(B6), 12205-12222.

Venegas, C., Cervetto, M., Astudillo, N., Espinoza, F. (2013). Carta Sierra Vaquillas Altas, Regiones de Antofagasta y Atacama. Servicio Nacional de Geología y Minería, Carta Geológica de Chile, Serie Geología Básica 159. 1 map at scale 1:100,000. Santiago, Chile.

Vezzoli, L., Tibaldi, A., Renzulli, A., Menna, M., Flude, S., (2008). Faulting-assisted lateral collapses and influence on shallow magma feeding system at Ollagüe volcano (Central Volcanic Zone, Chile–Bolivia Andes). J. Volcanol. Geotherm. Res. 171, 137–159.

Villa, V., Ramírez, C., Ferrando, R., Montecino, D., & Lienlaf, M. (2019). Geología de las áreas Salar Punta Negra y Cerro Sur Bayo, Región de Antofagasta. Servicio Nacional de Geología y Minería, Carta Geológica de Chile, Serie Geología Básica, 1.

Viramonte, J. G., Galliski, M. A., Saavedra, V. A., Aparicio, A., García-Cacho, G. L., & Escorza, C. M. (1984). El finivulcanismo básico de la depresión de Arizaro, provincia de Salta. IX Congreso Geolólgico Argentino, Actas, 3, 234-251

Watanabe, T., Koyaguchi, T., Seno, T., (1999). Tectonic stress controls on ascent and emplacement of magmas. J. Volcanol. Geotherm. Res. 91, 65–78.

Willemse, E. J. (1997). Segmented normal faults: Correspondence between three-dimensional mechanical models and field data. Journal of Geophysical Research: Solid Earth, 102(B1), 675-692.

Wörner, G., Moorbath, S., Horn, S., Entenmann, J., Harmon, R. S., Davidson, J. P., & Lopez-Escobar, L. (1994). Large-and fine-scale geochemical variations along the Andean arc of northern Chile (17.5–22 S). In Tectonics of the southern Central Andes (pp. 77-92). Springer, Berlin, Heidelberg.

Wörner, G., Mamani, M., & Blum-Oeste, M. (2018). Magmatism in the central Andes. Elements: An International Magazine of Mineralogy, Geochemistry, and Petrology, 14(4), 237-244.

Yañez, G., & Rivera, O. (2019). Crustal dense blocks in the fore-arc and arc region of Chilean ranges and their role in the magma ascent and composition: Breaking paradigms in the Andean metallogeny. Journal of South American Earth Sciences, 93, 51-66.

Zoback, M. L., & Magee, M. (1991). Stress magnitudes in the crust: constraints from stress orientation and relative magnitude data. Philosophical Transactions of the Royal Society of London. Series A: Physical and Engineering Sciences, 337(1645), 181-194.

Author contributions

Conceptualization: Diego Jaldin, Alessandro Tibaldi ; Methodology: Diego Jaldin, Daniela Espinoza, Karina Luengo, Alberto Santander; Formal analysis and investigation: Diego Jaldin, ; Writing - original draft preparation: Diego Jaldin; Writing - review and editing: Alessandro Tibaldi, Fabio Bonali; Laura Giambiagi, Elena Russo.

			Locations			Dinamyc Analisys (Angelier 1990)									
						σ1		σ2		σ3					
		Station	Longitude	Latitude	n	Trend	Plunge	Trend	Plunge	Trend	Plunge	φ	R'	Misfit deg	Stress Regimen
Lower-Middle Miocene	Sierra de Almeida Domain	011b	-68.55	-24.43	10	92	19	213	56	352	27	0.208	1.792	13.4	TP
		121	-68.67	-24.56	12	206	5	113	26	306	63	0.401	2.041	47.6	TP
		002a	-68.633	-24.528	22	71	9	168	37	329	51	0.151	2.151	15.8	TP
		005a	-68.634	-24.39	14	270	13	22	58	173	28	0.54	1.46	14.1	SS
		011a	-68.55	-24.43	21	15	74	247	10	155	12	0.635	0.635	29.1	PE
		012a	-68.589	-24.178	35	98	11	322	76	190	10	0.312	1.688	27.8	SS
		014a	-68.662	-24.205	28	233	17	325	8	80	71	0.798	2.798	9.7	RC
		106a	-68.5726	-24.35413	7	77	9	332	60	172	28	0.646	1.354	32.3	SS
		107a	-68.56452	-24.35299	30	71	4	330	69	162	20	0.704	1.296	35.3	SS
		114a	-68.49941	-24.25936	12	287	27	55	51	182	26	0.797	1.203	13	TT
		123a	-68.63	-24.57	30	204	15	297	9	57	72	0.77	2.77	28.4	RC
		123c	-68.63082	-24.57113	35	69	51	248	39	338	0	0.66	0.66	29	PE
		128a	-68.6272	-24.74756	5	85	19	328	53	186	30	0.305	1.695	3.9	SS
		129a	-68.48	-24.53	13	274	24	167	34	33	46	0.332	2.322	17	PC
	Aguas Calientes Domain	304a	-68.63811	-24.93094	14	88	25	259	65	357	4	0.216	1.784	19.8	TP
		305a	-68.64434	-24.9138	13	44	2	135	22	311	68	0.679	2.679	10.3	PC
		311a	-68.62682	-24.79809	5	261	5	360	56	168	33	0.483	1.562	29.6	SS
		317a	-68.61054	-24.83172	12	249	17	355	41	143	44	0.123	2.123	13.1	TP
		317b	-68.61054	-24.83172	5	35	10	130	26	285	62	0.604	2.604	8.9	PC
		309	-68.60199	-24.87342	11	90	2	184	62	360	27	0.507	1.493	7.2	SS
	Culampaja Domain	401a	-69	-24.965	18	104	16	196	8	310	72	0.532	2.532	26.3	PC
		401b	69	24.965	12	273	31	108	58	8	7	0.409	1.591	14.7	SS
		501a	-69.14504	-25.31058	15	111	8	201	5	324	80	0.423	2.423	23.3	PC
		518a	-68.98555	-25.61943	10	98	8	350	64	192	24	0.396	1.604	8	SS
		521	-68.98717	-25.70078	35	323	8	229	25	70	64	0.58	2.58	29.9	PC
Upper Miocene (8 to 4 Ma)	Sierra de Almeida Domain	116	-68.48	-24.38	7	297	13	34	30	187	57	0.349	2.349	18.5	PC
		114b	-68.49941	-24.25936	4	335	54	166	35	72	5	0.773	0.773	4.5	TT
		128b	-68.6272	-24.74756	8	344	23	167	67	75	1	0.508	1.492	14.8	SS
	Aguas Calientes Domain	311b	-68.62682	-24.79809	8	335	16	185	72	67	9	0.767	1.233	20.1	TT
		319	-68.4927	-24.89356	14	340	40	176	85	70	1	0.442	1.558	11.1	SS
		315	-68.56703	-24.929771	12	26	10	136	63	291	25	0.183	1.817	26.4	TP
		308	-68.61468	-24.88962	13	164	17	2	72	255	5	0.536	1.464	12	SS
		305b	-68.64434	-24.9138	10	325	9	59	18	210	68	0.404	2.404	23.7	PC
		304b	-68.63811	-24.93094	9	164	36	359	53	259	7	0.733	1.267	11.8	SS
		324b	-68.70157	-24.99567	5	338	59	124	26	222	15	0.637	0.637	10.5	PE
		318a	-68.55399	-24.96039	9	25	7	115	3	226	82	0.61	2.61	14.1	PC
		318b	-68.55399	-24.96039	5	137	55	7	24	266	24	0.649	0.649	19.8	PE
		314	-68.652955	-25.034307	7	146	9	54	13	269	74	0.281	2.281	20	PC
		312	-68.53379	-25.06734	9	162	1	253	26	69	64	0.518	2.518	11.2	PC
		313a	-68.55319	-25.07787	10	285	7	34	70	193	19	0.353	1.647	16.4	SS
		313b	-68.55319	-25.07787	5	355	3	251	78	86	11	0.617	1.383	13.3	SS
		320b	-68.62351	-25.1471	9	286	5	25	58	193	31	0.245	1.755	18.4	TP
	Culampaja Domain	501b	-69.14504	-25.31058	17	190	6	284	36	92	53	0.08	2.08	23.2	TP
		502	-69.14394	-25.31151	9	314	61	180	17	92	22	0.608	0.608	15.3	PE
		505	-69.10166	-25.33531	11	326	41	172	46	68	14	0.749	1.251	15.7	SS
		508a	-68.95632	-25.18706	11	314	14	102	73	222	9	0.979	1.021	8.6	TT
		508b	-68.95632	-25.18706	12	196	31	45	56	294	14	0.962	1.038	7.8	TT
		518b	-68.98555	-25.61943	11	163	70	296	6	1	19	0.476	0.476	40.1	PE
		515a	-68.83229	-25.4273	24	160	2	278	86	70	4	0.667	1.333	12.7	SS
		201a	-68.87	-24.79	9	258	20	165	9	52	68	0.322	2.322	25.7	PC
		201c	-68.87	-24.79	20	160	10	46	67	254	21	0.454	1.546	25.4	SS
Post-Pliocene (< 4 Ma)	Sierra de Almeida Domain	130a	-68.52	-24.55	11	21	11	186	79	290	3	0.883	1.167	5	TT
		126	-68.56	-24.67	20	24	21	130	35	270	48	0.273	2.273	12.7	PC
		107b	-68.56452	-24.35299	13	353	30	203	57	91	14	0.353	1.647	24.8	SS
	Aguas Calientes Domain	310	-68.615155	-24.867231	12	17	11	282	25	129	62	0.581	2.581	14.9	PC
		316	-68.652955	-25.034307	6	6	25	155	61	270	13	0.475	1.525	4.3	SS
		320a	-68.62351	-25.1471	19	18	9	227	79	108	5	0.151	1.849	23.4	TP
	Culampaja Domain	512	-68.80312	-25.3678	15	172	10	49	72	265	15	0.653	1.347	16.2	SS
		522	-68.689978	-25.715039	10	169	2	50	86	259	4	0.319	1.681	32.2	SS
		515b	-68.83229	-25.4273	10	36	56	226	33	133	5	0.615	0.615	8.9	PE
		514a	-68.79923	-25.44358	8	13	0	104	64	282	26	0.651	1.349	11.6	SS

Table 1. Trend and plunge of each principal stress axis (σ1, σ2, and σ3), ϕ Ratio, R' value and Misfit Angle. RC, Radial compressive, PC: Pure compressive, TP: Transpresive, PS: Pure Strike-slip, TT: Transtensive, PE: Pure extension, RC: Radial extension

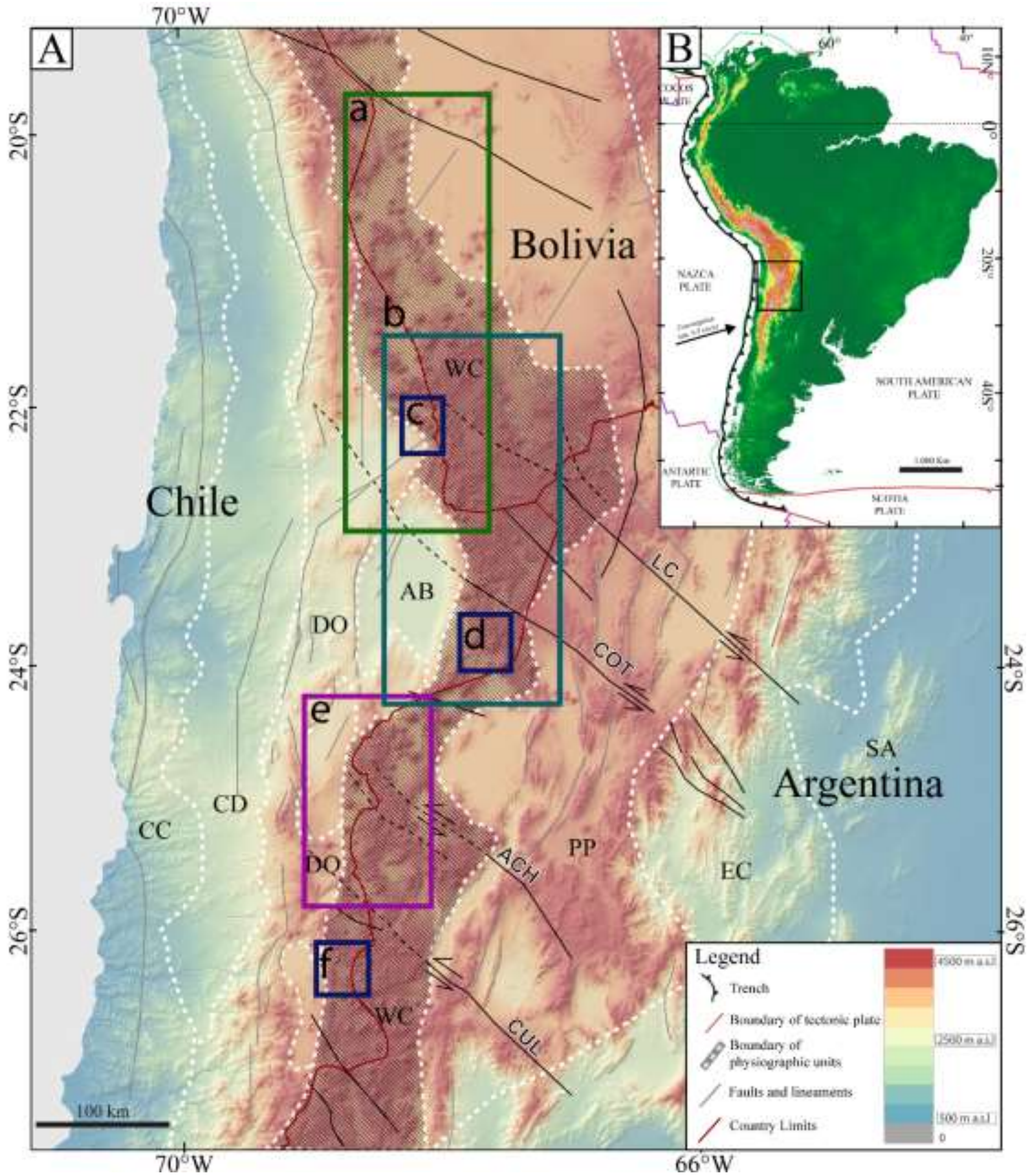

Figure 1. Location of the study area as related to morphotectonic provinces and regional main structures. A: Areas previously studied by other authors that have been integrated in the present work: (a) Tibaldi et al., (2009); (b) Tibaldi et al., (2017); (c,d,f) Giambiagi et al., (2016). (e) Study area of the present research with new structural and volcanic data. The main regional structures represented in the map are LC: Linzor Lineament; COT: Calama-Olacapato-El Toro Lineament; ACH: Archibarca Lineament; CUL: Culampaja Lineament. Morphotectonic provinces: CC: Coastal Cordillera; CD: Central depression; DO: Domeyko Range; AB: Pre-andean Basin; WC: Western Cordillera; PP: Altiplano-Puna Plateau; EC: Eastern Cordillera; SA: Sub-Andean range. Morpho-structural limits from Trumbull et al., (2006).

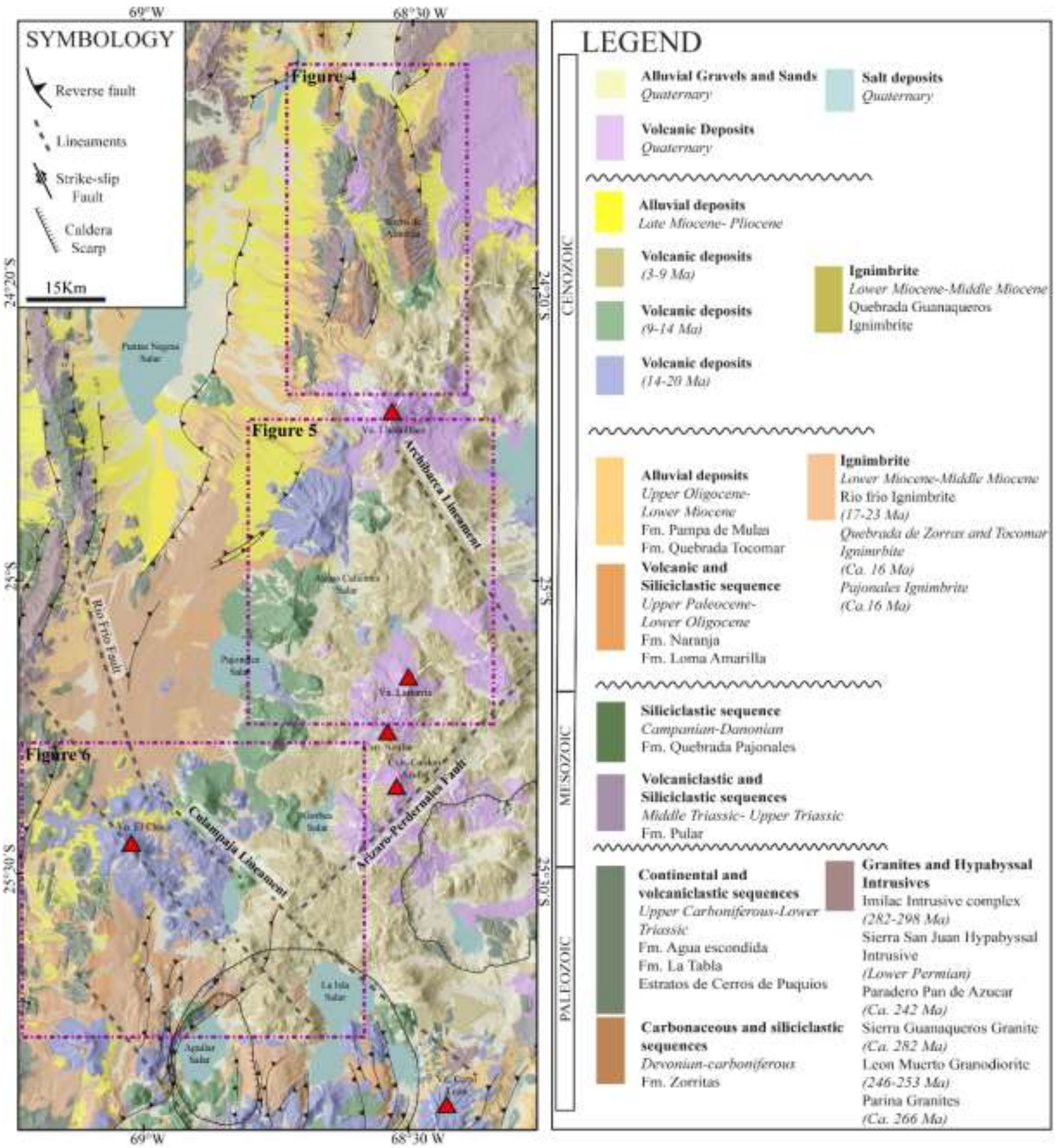

Figure 2. Simplified geological map of the study area with volcanic edifices divided by main time periods, based on Naranjo et al., 2013 a,b; Venegas et al., 2013; Gonzalez et al., 2015; Solari et al., 2017; Villa et al., 2019. Dashed boxes represent areas of detailed structural maps.

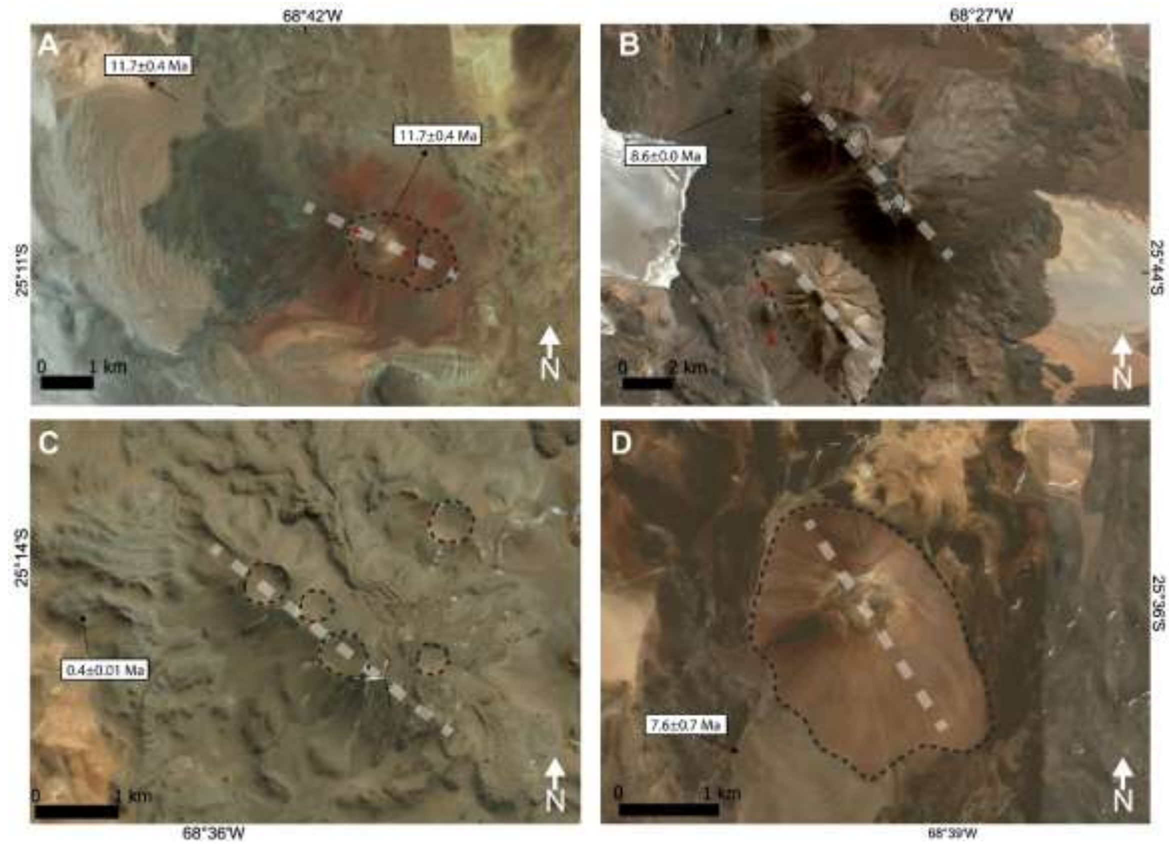

Figure 3. Google Earth images of some examples of volcanoes at which it has been possible to reconstruct the shallow magma-feeding fracture (dashed lines), based on: a) alignment of overlapping crater or b,c) eruptive centres, and azimuth of edifice elongation (d). Red arrow: directions of elongations of domes. Images from Google Earth, dating from Naranjo et al., (2013b).

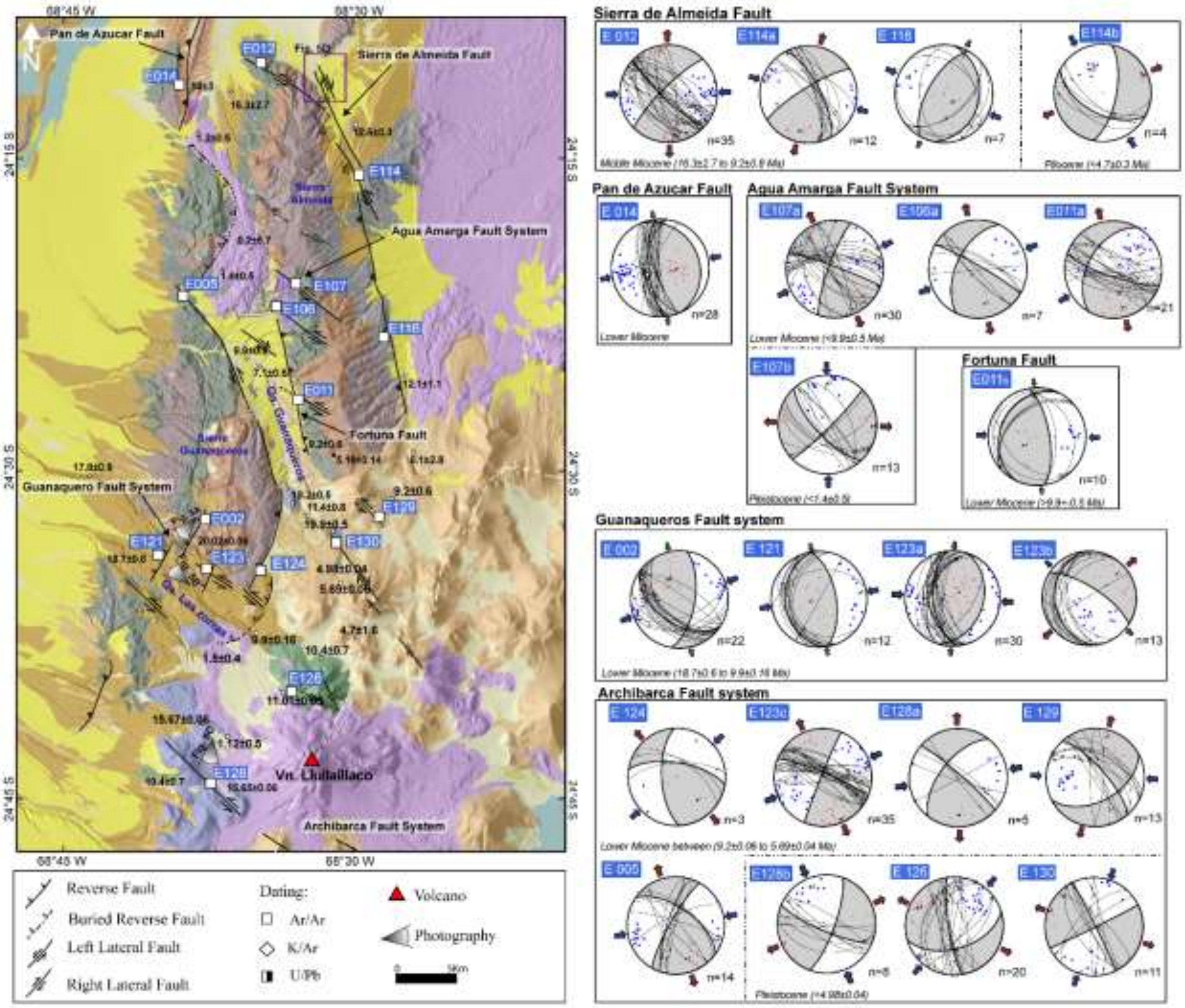

Figure 4. Structural map and kinematic analysis of the Sierra de Almeida domain. Positions of absolute ages are from Solari et al. (2017). E005; E012; E002 and E005 from Crignola 2002. Location in Figure 2.

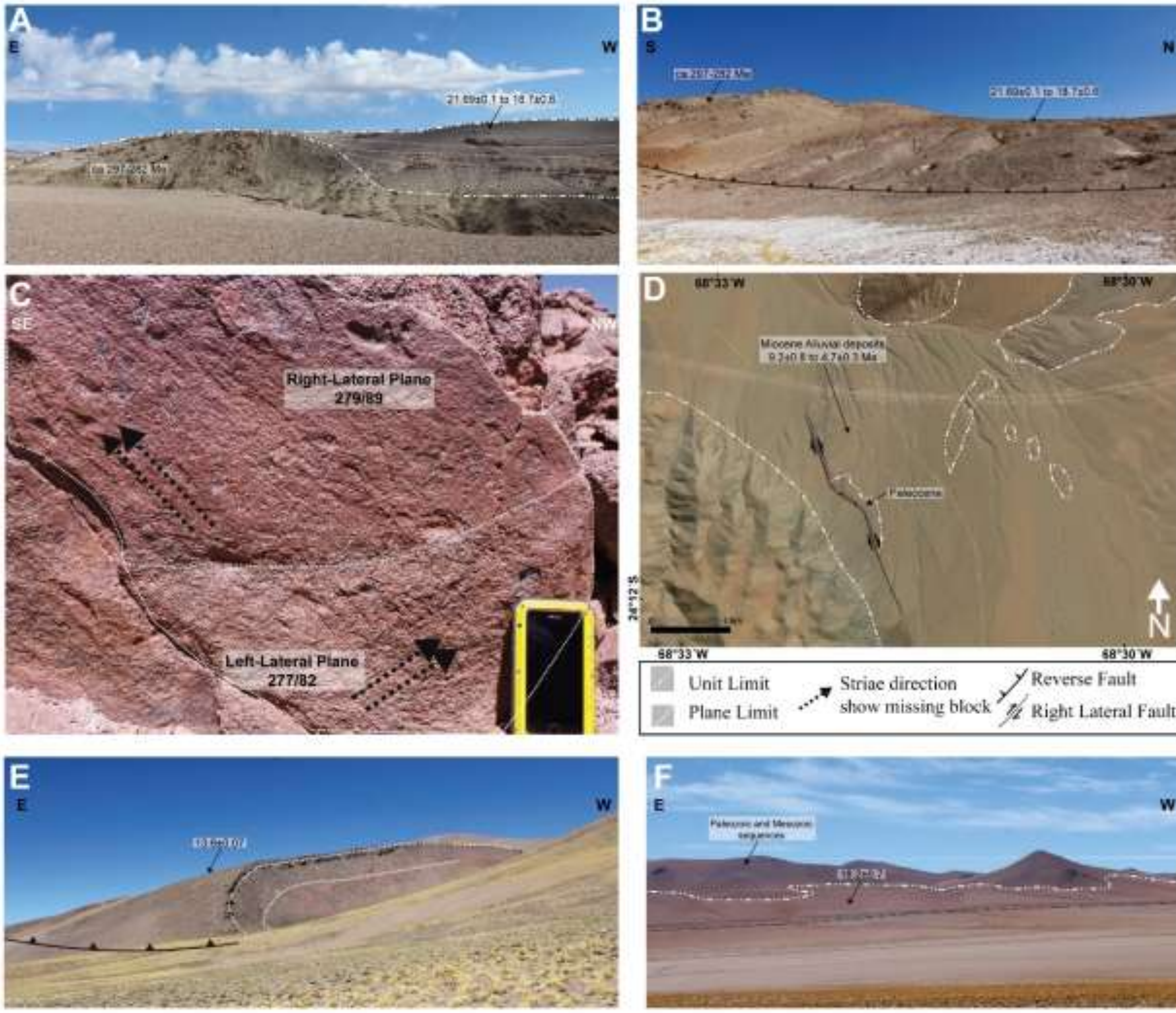

Figure 5. Field observations. A: Miocene alluvial sequence deposited in the back limb of a thrust fault that uplifted the Paleozoic basement, Location Fig. 4. B. Upper Oligocene-Lower Miocene alluvial deposits and pyroclastic sequence affected by a reverse Guanaqueros fault. C. Crosscutting relationships between two sets of striae with right- and left-lateral oblique reverse movement. D. Plan view of transcurrent deformations that affected the Miocene to Lower Pliocene gravels. E. Fold in the Lower Miocene volcanic deposits of the Aguas-Calientes volcano. F. Fault scarp affecting the Lower Miocene Rio Frio Ignimbrite.

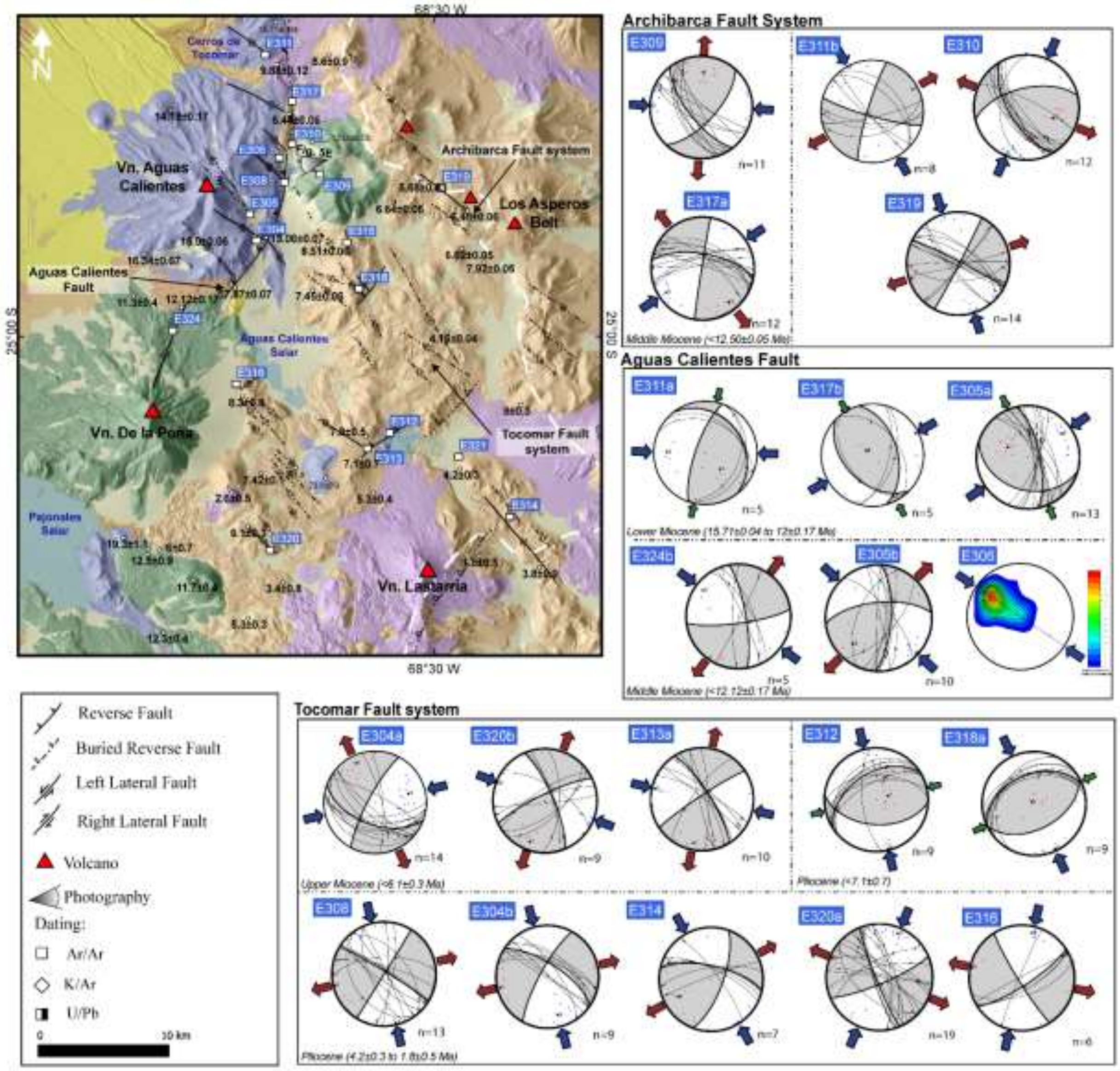

Figure 6. Structural map and kinematic analysis of the Aguas Calientes domain. Positions of absolute ages are taken from Naranjo et al. (2013b), and Villa et al. (2019). Location in Figure 2.

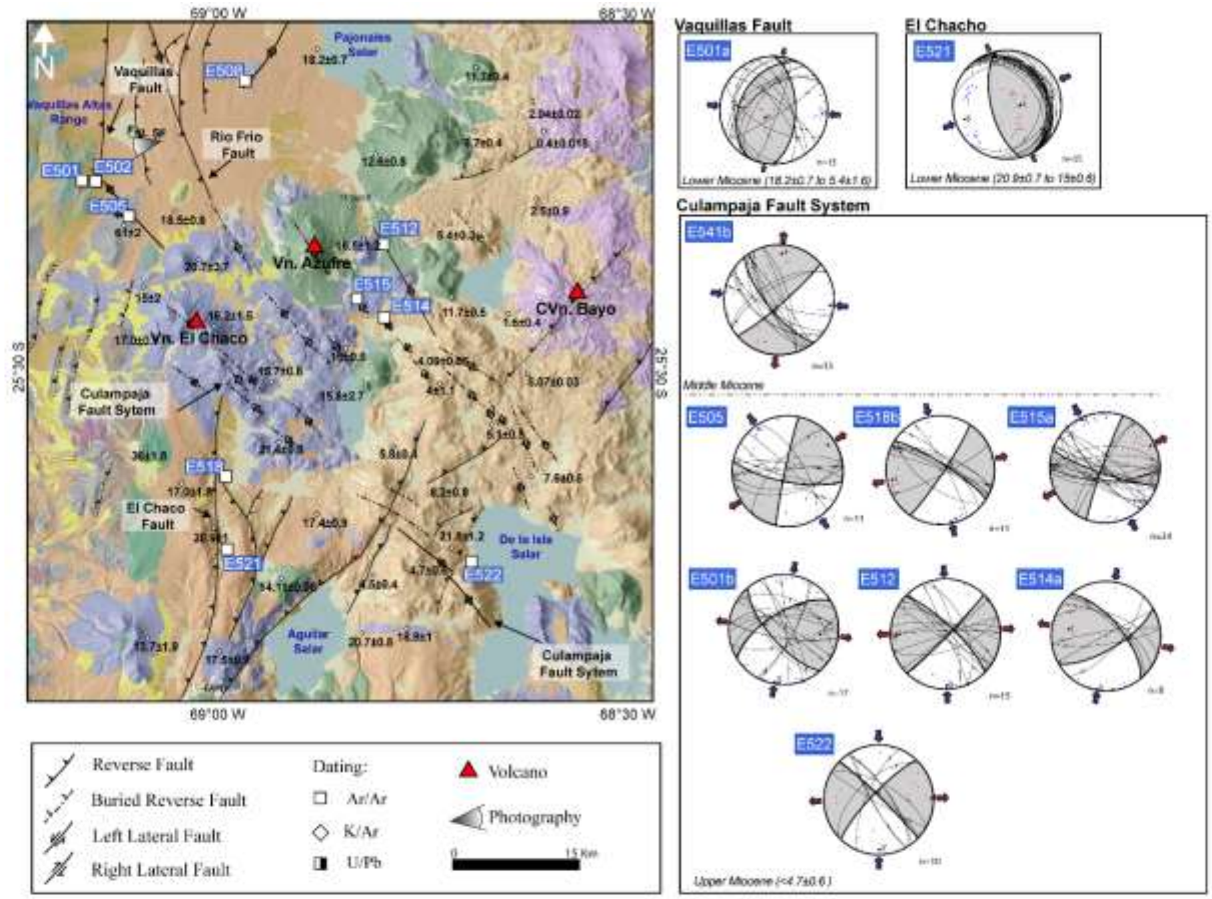

Figure 7. Structural map and kinematic analysis of Culampaja domain. Positions of absolute ages taken from Venegas et al. (2013) and Naranjo et al. (2013a). Location in Figure 2.

1269

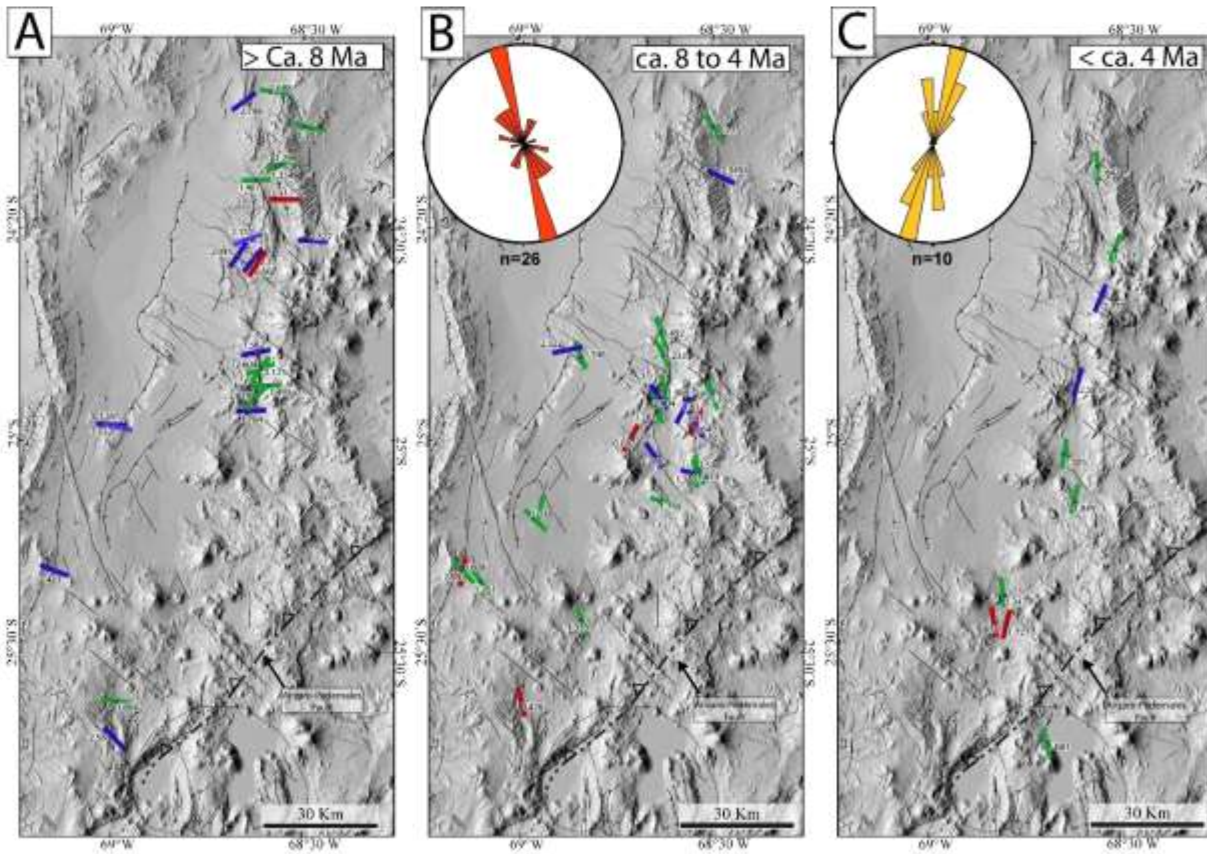

1270 **Figure 8.** Maps of stress tensors measured at Miocene-Quaternary faults in the study area and
1271 corresponding rose diagrams with the principal orientation of σ_{Hmax} axes. A: Lower to Middle Miocene
1272 (< 8 Ma); B: Upper Miocene (8-4 Ma), C: Post-Pliocene (< 4 Ma). Blue line: orientations of σ_{hmax} (σ_1)
1273 axes, compressive regime; Green line: orientations of σ_{Hmax} axes, strike-slip regimen; Red line: σ_{hmax}
1274 (σ_2), extensional regime. With box: R values.

1275

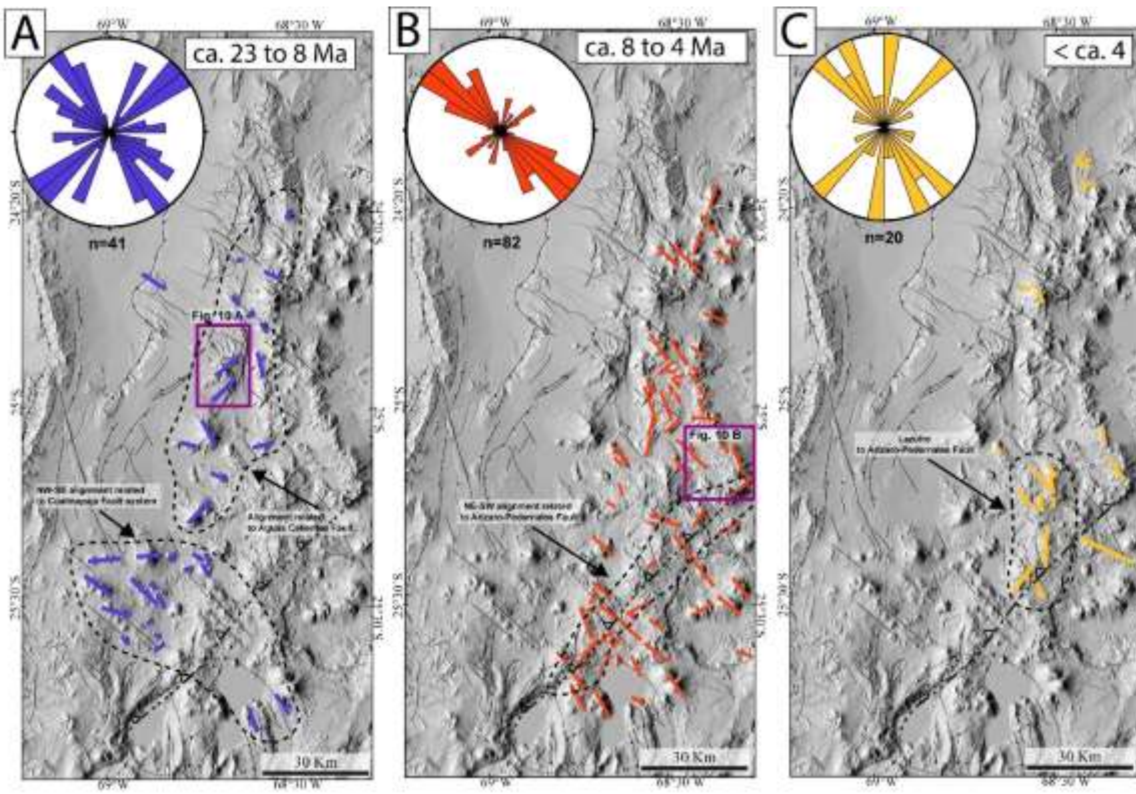

Figure 9. Maps of magma-feeding fractures, which should correspond to σ_{Hmax}, obtained by volcano morphometric characteristics measured at Miocene-Quaternary volcanoes in the study area, and corresponding rose diagrams with their main orientations. A: Lower to Middle Miocene (< 8 Ma), blue lines: orientations of σ_{Hmax}; B: Upper Miocene (8-4 Ma), red lines: orientations of σ_{Hmax}; C: Post-Pliocene (< 4 Ma), yellow lines: orientations of σ_{Hmax}.

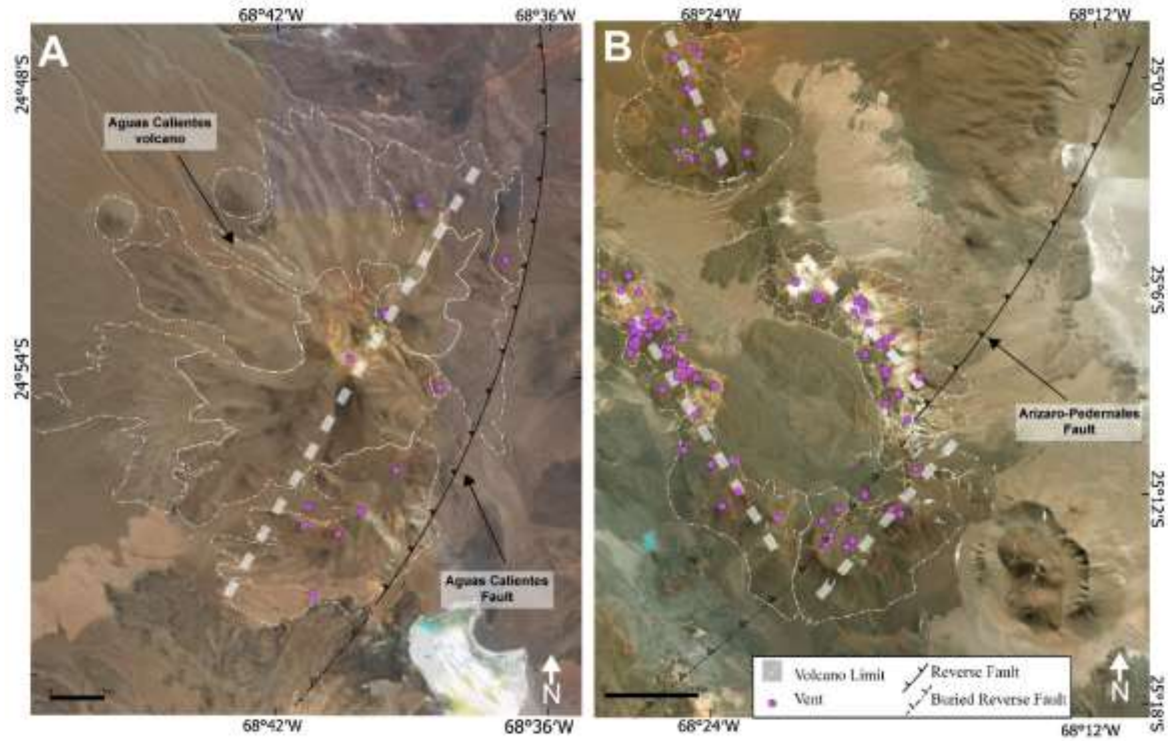

Figure 10. Examples of the relations between volcanoes and reverse faults of the same age. A: Aguas Calientes Volcano; B: Arizaro Volcano. Note that at both volcanoes, the vents located near or above the reverse fault trace are aligned parallel to the fault strike (NNE-SSW). In Figure B, vents located at greater distance from the reverse fault strike NW-SE. Locations in Figure 9. The basemap is given by Google Earth images.

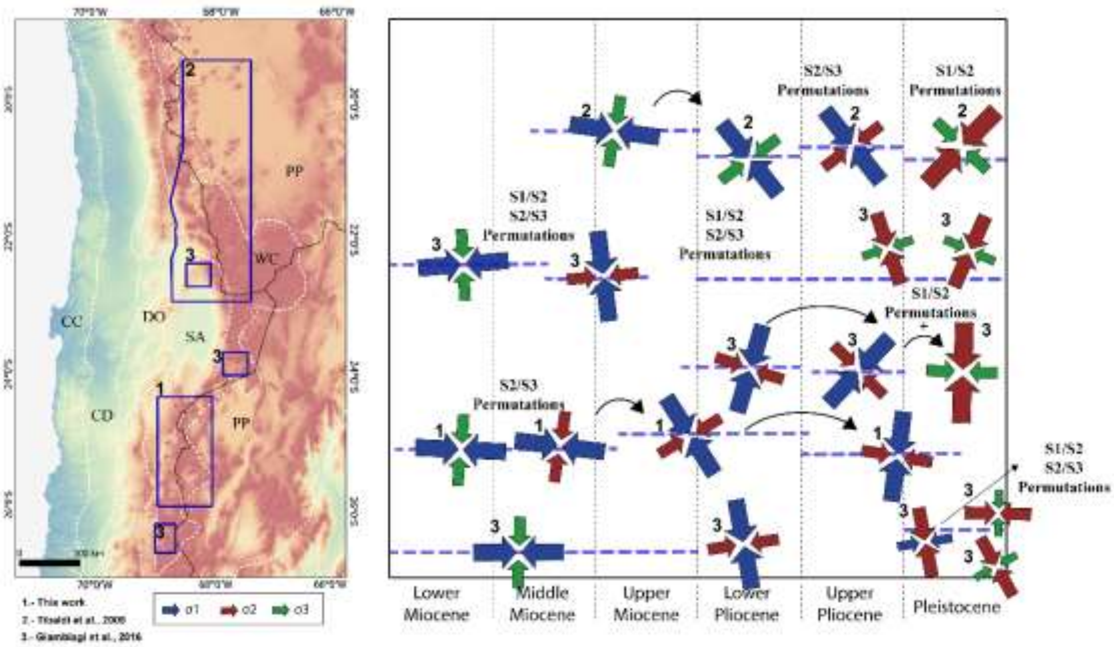

Figure 11. Correlations figure of stress tensors and stress regimes on the Western Cordillera from 20°S to 26°S. Left: map with distributions of correlated work. Right: shows the directions of stress tensor for Western cordillera. Blue boxes represent locations of compiled data. Data compiled from the present work (1), Tibaldi et al. (2009) (2), and Giambiagi et al. (2016) (3).

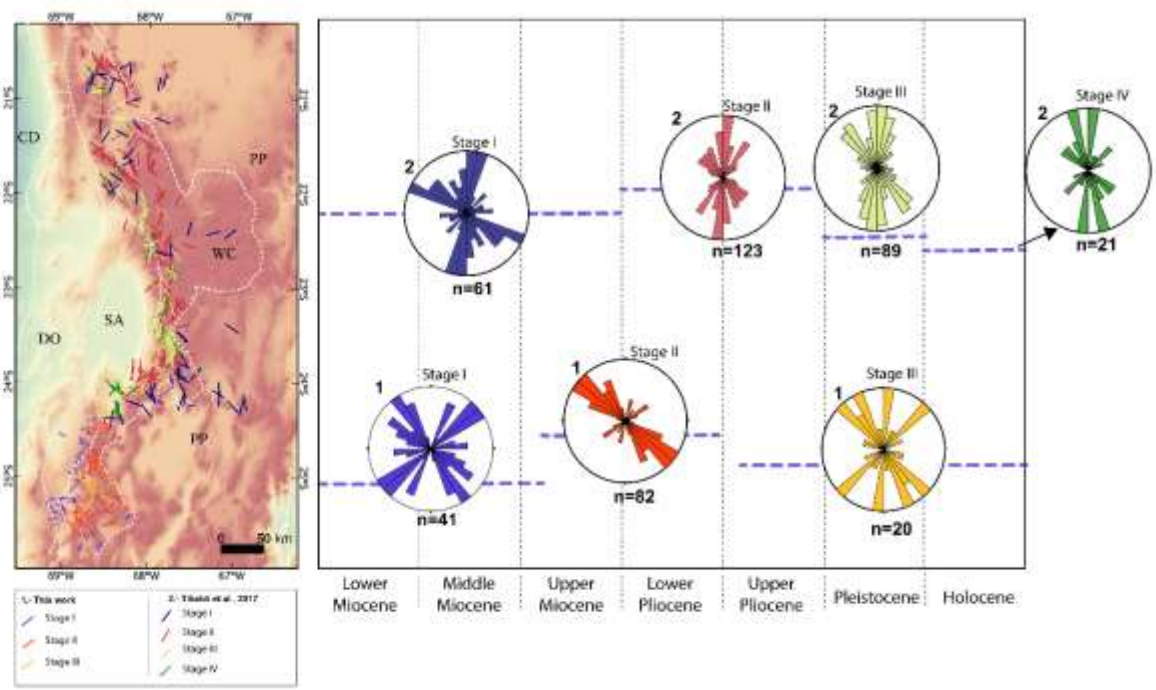

Figure 12. Figure summarizing resuming the various orientations of magma paths in the Western Cordillera (20°S to 26°S) expressed as rose diagrams in the different time periods. Data compiled from the present work (1) and from Tibaldi et al. (2017) (2).

Supplementary Information (S1)

Table 1. Trend and plunge of each principal strain axis from Linked Bingham Methods (λ1, λ2, and λ3), P and T axis. Strike and Dip of plane of solution from Linked Bingham Methods (Marret and Allmendinger, 1990). T: Thrust, L: Left-lateral, R: Right-Lateral, N: Normal.